
AN INFORMATION THEORETIC EVALUATION METRIC FOR STRONG UNLEARNING

Dongjae Jeon^{1,2*} Wonje Jeung^{1,2*} Taeheon Kim^{1,2} Albert No^{1†} Jonghyun Choi^{2†}

¹Yonsei University ²Seoul National University

{dongjae0324,specific0924,thkim0305,albertno}@yonsei.ac.kr
jonghyunchoi@snu.ac.kr

October 22, 2024

ABSTRACT

Machine unlearning (MU) aims to remove the influence of specific data from trained models, addressing privacy concerns and ensuring compliance with regulations such as the “right to be forgotten.” Evaluating strong unlearning, where the unlearned model is indistinguishable from one retrained without the forgetting data, remains a significant challenge in deep neural networks (DNNs). Common black-box metrics, such as variants of membership inference attacks and accuracy comparisons, primarily assess model outputs but often fail to capture residual information in intermediate layers. To bridge this gap, we introduce the Information Difference Index (IDI), a novel white-box metric inspired by information theory. IDI quantifies retained information in intermediate features by measuring mutual information between those features and the labels to be forgotten, offering a more comprehensive assessment of unlearning efficacy. Our experiments demonstrate that IDI effectively measures the degree of unlearning across various datasets and architectures, providing a reliable tool for evaluating strong unlearning in DNNs.

1 Introduction

Machine unlearning (MU) seeks to remove the impact of specific data samples from a trained model, addressing privacy issues such as “right to be forgotten” [Cao and Yang, 2015, Voigt and Von dem Bussche, 2017]. In addition to privacy, MU is also emerging as a tool to eliminate the influence of corrupted or outdated data used during training [Nguyen et al., 2022, Kurmanji et al., 2024]. The most straightforward approach to MU is *exact unlearning*, where the model is retrained from scratch, excluding the data that need to be forgotten. Although this method ensures complete data removal, it is computationally expensive and not scalable [Aldaghri et al., 2021, Bourtole et al., 2021, Yan et al., 2022]. Consequently, research has shifted towards *approximate unlearning*, which aims to replicate the effects of retraining in a more efficient manner.

The goal of MU is to create an unlearned model that is indistinguishable from a model retrained from scratch, referred to as strong unlearning. This objective has become particularly crucial with the rise of open-source models like Stable Diffusion [Rombach et al., 2022] and LLaMA [Touvron et al., 2023], which are widely used and fine-tuned by various users. For unlearning algorithms to be practically useful, they must be capable of fully eliminating traces of private data and preventing potential exploitation. While (ϵ, δ) -certified unlearning methods [Zhang et al., 2024, Mu and Klabjan, 2024] provide theoretical guarantees, they are often impractical for large-scale models. As a result, most approximate unlearning methods rely on heuristic approaches, lacking formal guarantees. Thus, these methods must undergo empirical evaluation to demonstrate their effectiveness.

However, current evaluations, primarily based on black-box approaches such as membership inference attacks (MIA) [Shokri et al., 2017, Carlini et al., 2022] and accuracy comparisons, focus on output similarity rather than internal

*Equal contribution. The authors are listed in alphabetical order.

†Corresponding authors

model changes. Although these metrics may capture weak unlearning [Fan et al., 2023, Liu et al., 2024, Chundawat et al., 2023b, Foster et al., 2024, Chen et al., 2023], they may not be sufficient for assessing strong unlearning. In this work, we investigate whether relying solely on outputs can truly reflect complete influence removal, considering that outputs can be superficially adjusted without impacting internal representations [Kirichenko et al., 2023].

Surprisingly, our experiments reveal that even minimal changes to the model, such as modifying only the final layer while preserving all information in the intermediate layers, can still satisfy black-box evaluation metrics, exposing their limitations in assessing strong unlearning. This finding also raises critical concerns about whether current MU methods genuinely achieve information removal comparable to retraining from scratch, despite yielding similar model outputs.

Consequently, motivated by the Information Bottleneck principle [Tishby et al., 2000, Tishby and Zaslavsky, 2015], which interprets deep neural network training as regulating the flow of information through successive layers, we introduce the **information difference index (IDI)**, a novel white-box metric designed to quantify residual information in intermediate layers after unlearning. IDI measures the mutual information [Shannon, 1948] between intermediate features and the forgetting labels, providing an interpretable value to assess the effectiveness of unlearning algorithms.

We observe that IDI remains robust, delivering consistent results despite the inherent stochasticity of the unlearning process, and is model-agnostic, making it adaptable to various model architectures. Furthermore, IDI enables detailed evaluation and comparison of MU methods without requiring access to the entire training dataset, which is especially advantageous for large-scale datasets like ImageNet-1K and complex models such as Vision Transformers (ViT). To the best of our knowledge, IDI is the first practical and reliable white-box metric developed for evaluating unlearning quality, a critical aspect that remains underexplored in the unlearning field.

Through the application of IDI, we discovered that many recent MU methods still retain substantial residual information within their intermediate layers, even when they perform well on black-box metrics. This residual information can be leveraged to recover forgotten data with minimal effort, indicating that several methods may not fully meet the core objective of MU. These findings highlight the value of incorporating white-box metrics like IDI to provide a more comprehensive evaluation, ensuring that unlearning efforts truly eliminate all relevant information.

Building on the insights gained from IDI, we introduce **COLapse-and-Align (COLA)**, a method specifically designed to address the residual information related to the forgetting data in unlearning processes. COLA follows a two-step approach: first, it applies supervised contrastive loss [Khosla et al., 2020] to collapse feature-level representations associated with the forgetting data; second, it fine-tunes the entire model to align the parameters. Despite its simplicity, COLA serves as a useful benchmark, demonstrating measurable improvements in IDI scores compared to other methods on datasets such as CIFAR-10, CIFAR-100, and ImageNet-1K, as well as architectures like ResNet-18, ResNet-50, and ViT. Notably, COLA achieves this without access to the full training dataset, unlike several existing methods. The ability of IDI to capture COLA’s impact on intermediate features further underscores its value as a robust efficacy metric.

We summarize our contributions as follows:

1. We identify the limitations of existing black-box metrics, which focus on model outputs and fail to detect residual information in intermediate layers, thus inadequately assessing strong unlearning.
2. We introduce the information difference index (IDI), an interpretable metric based on information theory that measures the mutual information between intermediate features and the forgetting labels, offering a more comprehensive evaluation of unlearning efficacy.
3. We demonstrate the effectiveness of IDI through extensive experiments across diverse datasets such as CIFAR-10, CIFAR-100, and ImageNet-1K, and model architectures including ResNet and ViT, validating its robustness and applicability in various contexts.
4. Using the COLapse-and-Align (COLA) method as a benchmark, we show that IDI effectively captures residual information in intermediate features, demonstrating its value as a reliable metric for evaluating unlearning quality and highlighting the need for white-box metrics in the field.

2 Problem Statement and Preliminaries

2.1 Problem Statement

Let $\mathcal{D} = \{(x_i, y_i)\}_{i=1}^N$ denote the training dataset, which consists of N samples, each represented by an image-label pair (x_i, y_i) . In a supervised learning setup, we partition the dataset into two subsets: the *forget set* \mathcal{D}_f , which comprises instances to be forgotten, and *retain set* $\mathcal{D}_r = \mathcal{D} \setminus \mathcal{D}_f$, containing instances to be retained. The initial model, θ_o (referred to as **Original**), is trained on the complete dataset \mathcal{D} via empirical risk minimization. The unlearned model, θ_u , is the

result of modifying Original through a specific unlearning algorithm that aims to remove influence of \mathcal{D}_f . The objective of machine unlearning (MU) is to ensure that the unlearned model θ_u closely approximates the model retrained from scratch exclusively on \mathcal{D}_r (referred to as **Retrain**). The two models should be indistinguishable, meaning the unlearned model should completely remove the influence of \mathcal{D}_f , as if that data had never been part of the training process. Both the Original and Retrain models use the same training methodology, differing only in their datasets: \mathcal{D} for Original and \mathcal{D}_r for Retrain.

MU is often studied in the context of image classification [Shaik et al., 2023, Nguyen et al., 2022], where it is typically classified into two scenarios based on the nature of the forget set: *class-wise forgetting*, where all samples from a specific class are targeted, and *random data forgetting*, where samples are selected indiscriminately across all classes.

Throughout the paper, within a given model θ , we define the **head** as the last few layers responsible for classification; typically one to three linear layers. The **encoder**, on the contrary, encompasses the remainder of the network, which usually consists of convolutional layers or transformer encoders.

2.2 Preliminaries

Machine Unlearning (MU). Exact unlearning, which involves creating Retrain, guarantees the information removal from the forget set but is computationally expensive [Bourtoule et al., 2021, Yan et al., 2022, Aldaghri et al., 2021, Brophy and Lowd, 2021]. To address this, approximate unlearning methods have been developed, focusing on efficiency rather than strict theoretical guarantees. Specifically, strong unlearning, where the unlearned model is indistinguishable from Retrain, has been explored through the application of differential privacy (DP) [Dwork and Roth, 2014] inspired techniques, which aim to achieve parameter-level indistinguishability [Dwork and Roth, 2014, Ginart et al., 2019, Neel et al., 2021, Sekhari et al., 2021, Ullah et al., 2021, Guo et al., 2019]. However, applying these techniques in deep neural networks (DNNs) remains challenging due to their vast number of parameters and non-convex loss landscapes [Qiao et al., 2024]. As a result, research has shifted towards proposing heuristic methods and empirically evaluating them by comparing the behavior of the unlearned model with that of Retrain. Recent studies typically assess the similarity of model outputs (*i.e.*, predictions), using weak unlearning as a practical proxy for strong unlearning [Xu et al., 2023]. While empirically ensuring strong unlearning is challenging, it is critical for deploying unlearning algorithms to meet legal requirements like GDPR [Voigt and Von dem Bussche, 2017], the “right to be forgotten”, and prevent retention of sensitive data, particularly with the growing use of open-source models like CLIP [Radford et al., 2021], Stable-Diffusion [Rombach et al., 2022], and LLaMA [Touvron et al., 2023], where data could unintentionally persist and be exploited.

Evaluation Criteria in MU. As the goal of MU is to remove the influence of specific data while preserving the others, the unlearning algorithms are typically evaluated on three criteria: *Efficacy*, *Accuracy*, and *Efficiency* [Hayes et al., 2024]. Efficacy measures how closely the unlearned model approximates Retrain, which is key to unlearning quality. Accuracy ensures task performance remains intact after unlearning, while efficiency ensures the unlearning process is faster than retraining.

Accuracy and efficiency can be easily evaluated using existing metrics. Accuracy consists of three categories: *unlearning accuracy* (UA), *remaining accuracy* (RA), and *testing accuracy* (TA). UA measures performance on \mathcal{D}_f as $UA(\theta_u) = 1 - \text{Acc}_{\mathcal{D}_f}(\theta_u)$, RA on \mathcal{D}_r as $RA(\theta_u) = \text{Acc}_{\mathcal{D}_r}(\theta_u)$, and TA measures generalization to unseen data as $TA(\theta_u) = \text{Acc}_{\mathcal{D}_{test}}(\theta_u)$. Performance levels comparable to Retrain across these metrics indicate better unlearning. In terms of efficiency, *runtime efficiency* (RTE) measures the time an algorithm takes to complete unlearning, with lower RTE indicating more efficient unlearning [Fan et al., 2023, Liu et al., 2024, Foster et al., 2024].

However, assessing unlearning efficacy, or determining whether the unlearned model has fully removed the influence of specific data to the same extent as Retrain, remains a significant challenge in complex DNNs. From a practical standpoint, recent studies often rely on empirical evidence for evaluation, with metrics generally divided into two categories: *black-box* metrics, which focus solely on model outputs (*i.e.*, predictions), and *white-box* metrics, which examine internal dynamics such as parameters, gradients, and features. While black-box metrics are typically used due to their convenience, no universally accepted standard exists, leaving room for more reliable assessment.

Black-box Efficacy Metrics. Variants of membership inference attacks (MIA) [Shokri et al., 2017, Carlini et al., 2022] are the most widely used black-box metrics [Shen et al., 2023, Kim et al., 2024, Fan et al., 2023, Liu et al., 2024, Foster et al., 2024]. MIA determines whether specific data were part of the training set by training an auxiliary classifier, with low success rates on the forget set that are close to those of Retrain being preferred. It is worth noting that recent works often use a combination of UA, RA, TA, MIA and RTE as metrics for evaluating unlearning performance across the three criteria [Chen et al., 2023, Kim et al., 2024, Liu et al., 2024, Fan et al., 2023], collectively referred to as the ‘full-stack’ evaluation scheme [Liu et al., 2024, Fan et al., 2023]. Other metrics, such as activation distance and

Jensen-Shannon divergence (JSD), compare the output logits between the unlearned model and Retrain [Chundawat et al., 2023b]. Additionally, time-based metrics like Anamnesis Index (AIN) [Chundawat et al., 2023a, Tarun et al., 2023a] and relearn time (RT) [Tarun et al., 2023b, Golatkar et al., 2020a,b, 2021] measure the time (or epochs) required for the unlearned model to regain performance on the forget set. While black-box metrics are widely adopted for their convenience, they have inherent limitations. By focusing solely on model outputs and overlooking internal behaviors, these metrics fail to indicate whether the unlearned model has completely removed the influence of the forgetting data, which is critical for assessing strong unlearning. In Section 3, we show that these metrics can be misleading, often suggesting successful unlearning even when residual information from the forget set remains within the model.

White-box Efficacy Metrics. In contrast, white-box metrics offer a more detailed evaluation by analyzing internal model dynamics to track residual influence. Previous studies have measured parameter-wise distances (e.g., ℓ_2 -distance, KL-divergence) between the unlearned model and Retrain [Golatkar et al., 2020a, Wu et al., 2020]. However, this approach is computationally expensive and unreliable due to the inherent randomness in DNN training [Hayes et al., 2024, Goel et al., 2022]. Becker and Liebig [2022] proposed a Fisher information based metric, but their experimental results were inconsistent with theoretical intuition. Graves et al. [2021] applied model inversion attacks to reconstruct images from the forget set, but this method relies on qualitative comparisons, making it difficult to compare across different algorithms. Although robust white-box metrics are currently lacking and challenging to develop, they are crucial for validating approximate methods, which often lack guarantees of complete information removal. Without such metrics, these methods cannot be trusted in privacy-sensitive applications that demand a high level of confidence in information removal. To address this critical need, our work proposes a reliable and practical white-box metric.

3 Rethinking the Evaluation of Unlearning Efficacy

3.1 Head Distillation: Simple Technique Challenges Black-box Metrics

In this section, we reveal the limitations of commonly used black-box efficacy metrics by applying our simple unlearning technique to a single-class forgetting task. We reveal how these metrics can misrepresent unlearning efficacy by overlooking residual information in intermediate features, even when the model’s output appears similar to that of Retrain.

Drawing inspiration from the teacher-student framework [Chundawat et al., 2023b, Kurmanji et al., 2024], our strategy, termed **head distillation (HD)**, employs logit distillation from Original θ_o . Specifically, the unlearned model θ_u is initialized from θ_o with the encoder frozen and only the head remaining trainable. During the unlearning process, the head is finetuned on training dataset \mathcal{D} using KL-divergence loss [Hinton et al., 2015] to follow the masked output from θ_o , where the logit for the forgetting class is set to negative infinity while preserving the logits for the remaining classes, as shown in Figure 1. This approach enables θ_u to mimic a pseudo-retrained model, as the masked logits closely resemble those of Retrain. By aligning the output behavior with that of Retrain, HD aims to simulate the desired unlearning effect.

We conducted experiments using the CIFAR-10 [Krizhevsky, 2009] dataset and the ResNet-18 architecture [He et al., 2016], where the head consists only of a single linear layer. To evaluate *efficacy*, we used a widely adopted black-box metric, membership inference attack (MIA) and Jensen-Shannon divergence (JSD). Additionally, we measured unlearning accuracy (UA), testing accuracy (TA) and run-time efficiency (RTE) for *accuracy* and *efficiency*. For more details on these metrics, please refer to Appendix B.1. We compared HD to recent approximate MU methods, including FT, RL [Golatkar et al., 2020a], GA [Thudi et al., 2022], ℓ_1 -sparse [Liu et al., 2024], and SALUN [Fan et al., 2023]. Details on the baselines can be found in Appendix B.2.

Figure 2 presents the experimental results. Despite its simplicity, HD exhibits remarkable performance across black-box efficacy metrics. In particular, HD outperforms all other methods in MIA and ranks second in JSD. Notably, HD achieves this level of performance in just 6.2 seconds, which is approximately 30 to 60 times faster than competing methods. Furthermore, HD maintains comparable results in testing accuracy (TA), effectively preserving task performance. Note that all methods achieved perfect unlearning accuracy (100% UA), which we omitted from Figure 2.

The experimental results indicate that HD performs exceptionally well across all black-box evaluation metrics. However, its validity as an effective MU algorithm warrants closer examination. The primary issue is that HD closely resembles

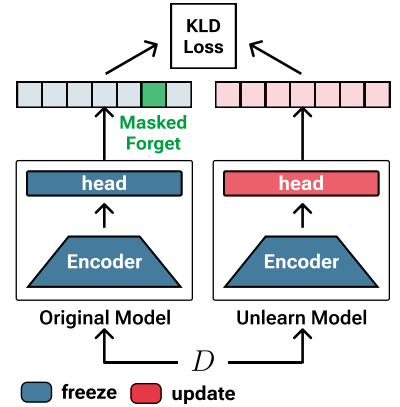


Figure 1: Overview of head distillation (HD): Original distills knowledge into the unlearn model’s head by masking the forgetting class logit, with the encoder kept frozen.

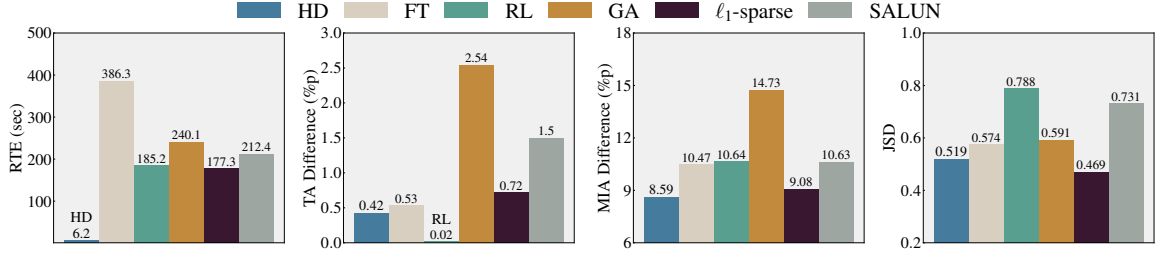


Figure 2: Performance of six methods (HD, FT, RL, GA, ℓ_1 -sparse, SALUN) on (CIFAR-10, ResNet-18), evaluated in efficiency (RTE), accuracy (TA), and efficacy (MIA, JSD). For TA, MIA, and JSD, lower differences from Retrain are preferred, indicating closer similarity to Retrain.

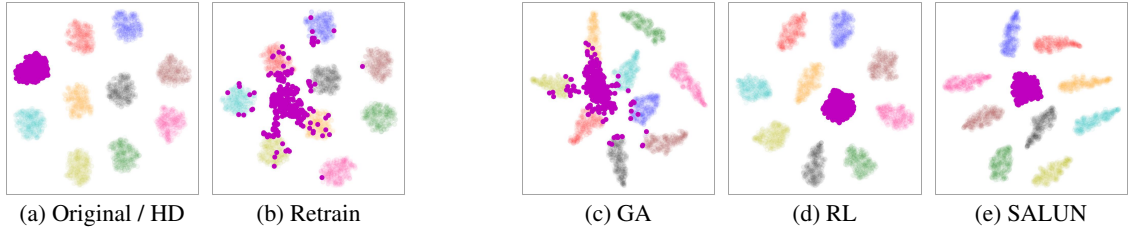


Figure 3: t-SNE visualizations of encoder outputs for Original, Retrain, and unlearned models from three MU methods (GA, RL, SALUN) on single-class forgetting with (CIFAR-10, ResNet-18). In each t-SNE plot, features of the forgetting class are represented in purple. Original and HD have identical feature distribution as they share the same encoder.

Original θ_o , with changes limited to the single-layer head, while the encoder remains identical to θ_o . Consequently, all intermediate features related to the forget set are retained. This raises a critical question:

*Do black-box metrics truly capture the unlearning quality,
or are they misled by superficial changes while deeper information persists?*

3.2 Residual Information of Forgetting Data: Limitations of Black-box Assessments for Unlearning Efficacy

To address the above question, we conducted two analyses on recent unlearning methods to determine whether they internally remove information from the forget set, despite their strong performance on black-box efficacy metrics. We note that both analyses are performed on the unlearned models using the same experimental setting discussed in Section 3.1.

We start with a qualitative analysis using t-SNE [van der Maaten and Hinton, 2008] visualizations of intermediate features from model encoders to investigate how Retrain differs from Original and to analyze the internal behavior of different unlearning algorithms, as shown in Figure 3. Figure 3b reveals the scattered distribution of the features corresponding to the forgetting class (represented in purple) in Retrain. These features are dispersed across multiple clusters, indicating the model’s difficulty in extracting coherent information from the forgetting class. This scattering reflects an ideal outcome of strong unlearning, suggesting that the unlearned model has successfully ‘forgotten’ how to represent meaningful semantic information from the forget set.

Notably, while the features from GA [Thudi et al., 2022] appear scattered in a manner similar to Retrain, the features from RL [Golatkar et al., 2020a] and SALUN [Fan et al., 2023] closely resemble those of Original. As expected, HD, which shares the same encoder as Original, produces t-SNE results identical to it. These findings indicate that several unlearned models still retain a significant capacity to recognize the forgetting class, distinguishing them from Retrain.

To further examine the residual influence of unlearned models, we conducted a follow-up experiment inspired by time-based metrics (e.g., [Chundawat et al., 2023a]). This experiment explores whether unlearned encoders can recover forgotten information with minimal data. Specifically, we replaced the heads of all unlearned models, including Retrain and Original, with randomly initialized ones. We then froze all the encoders and trained these new heads using \mathcal{D}' , a small subset (only 2% of the total) of \mathcal{D} consisting of randomly selected samples.

After training, we evaluated the accuracy of the new models on the forget test data. Surprisingly, as shown in Figure 4, while the retrained head of Retrain achieves no more than 41% accuracy, the heads from certain methods, like Bad-T, SALUN, and RL exhibit over 82% accuracy. Notably, the high accuracy observed in SALUN and RL corresponds to the clustered t-SNE plots in Figure 3.

The results from the above analyses demonstrate that unlearned models across various MU algorithms retain substantial residual influence from the forget set internally, unlike Retrain. This highlights incomplete unlearning in those approximate methods. However, a critical concern is that commonly used black-box assessments fail to detect these underlying residuals. If unlearning efficacy metrics cannot ensure strong unlearning, as clearly shown in our results, the reliability of approximate unlearning algorithms, which often lack theoretical guarantees, becomes questionable in real-world applications. Therefore, developing practical white-box approaches that consider internal model behaviors is essential to achieving the fundamental goal of unlearning.

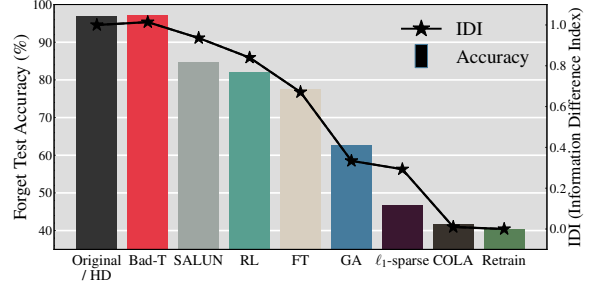


Figure 4: Forget test accuracy and IDI (our metric) for Original, Retrain, and seven MU methods, including COLA (our method), after head retraining with unlearned encoders (fixed) using 2% of \mathcal{D} in (CIFAR-10, ResNet-18).

4 An Information Theoretic Metric For Unlearning Efficacy Using Intermediate Features

Current MU efficacy evaluations, which rely primarily on black-box metrics, overlook residual information in intermediate layers, as shown in Section 3. To address this, we measure residual information in the intermediate features of unlearned models using mutual information. Building on this, we propose a novel white-box metric, IDI, that goes beyond output-based evaluations.

4.1 Quantifying Residual Information with Mutual Information

To quantify the relationship between high dimensional intermediate features and data labels, we utilize Shannon’s mutual information (MI), a robust measure that effectively captures variable dependencies across various dimensional complexities. For an input \mathbf{X} , let $\mathbf{Z}_\ell^{(u)}$ and $\mathbf{Z}_\ell^{(r)}$ denote the features from the ℓ -th layer of the total L -layer encoder in the unlearned model and Retrain, respectively. Let Y be a binary label, where $Y = 1$ indicates that the input \mathbf{X} belongs to the forget set, and $Y = 0$ otherwise. We measure the MI, denoted as $I(\mathbf{Z}_\ell; Y)$, across each layer from 1 to L , to determine whether intermediate features retain information about the forget set. To estimate MI, we use the InfoNCE loss [Oord et al., 2018]. InfoNCE is widely used in MI estimation of DNNs and shown to be robust and effective [Radford et al., 2021, Jia et al., 2021].

Given a batch of size K , $\{(U^{(k)}, V^{(k)}) : 1 \leq k \leq K\}$, sampled from a joint distribution $P_{U,V}$, where U and V are random variables, the InfoNCE loss [Poole et al., 2019] is defined as follows:

$$\mathcal{L}_{\text{NCE}}(U, V, \nu, \eta) = \frac{1}{K} \sum_{k=1}^K \log \frac{\exp(f_\nu(U^{(k)})^\top g_\eta(V^{(k)}))}{\frac{1}{K} \sum_{k'=1}^K \exp(f_\nu(U^{(k)})^\top g_\eta(V^{(k')}))},$$

where f_ν and g_η are critic functions parameterized as neural networks with parameters ν and η . This neural network parameterization is inspired by Radford et al. [2021], which demonstrated the effectiveness of using neural networks to model complex relationships in contrastive learning.

The InfoNCE loss serves as a lower bound on the MI between U and V . In fact, the maximum value of the InfoNCE loss, when using the joint critic functions, equals the mutual information:

$$I(U; V) = \max_{\nu, \eta} \mathcal{L}_{\text{NCE}}(U, V, \nu, \eta).$$

Thus, to estimate the mutual information, we maximize the InfoNCE loss over the parameters ν and η . By leveraging the flexibility of neural networks, we can effectively capture the underlying structure of the data and accurately quantify the amount of shared information between the variables U and V .

To estimate mutual information (MI) for each layer in the network, we design separate critic functions for every layer, denoted as f_{ν_ℓ} and g_{η_ℓ} . The function g_{η_ℓ} , which handles the binary variable Y , is straightforward, using a trainable d -dimensional vector to select $g_{\eta_\ell}(0)$ or $g_{\eta_\ell}(1)$ based on the label. In contrast, f_{ν_ℓ} is more complex, particularly in the earlier layers, where it captures information about Y from the raw features \mathbf{Z}_ℓ . Earlier features are harder to interpret, while later, refined ones are easier.

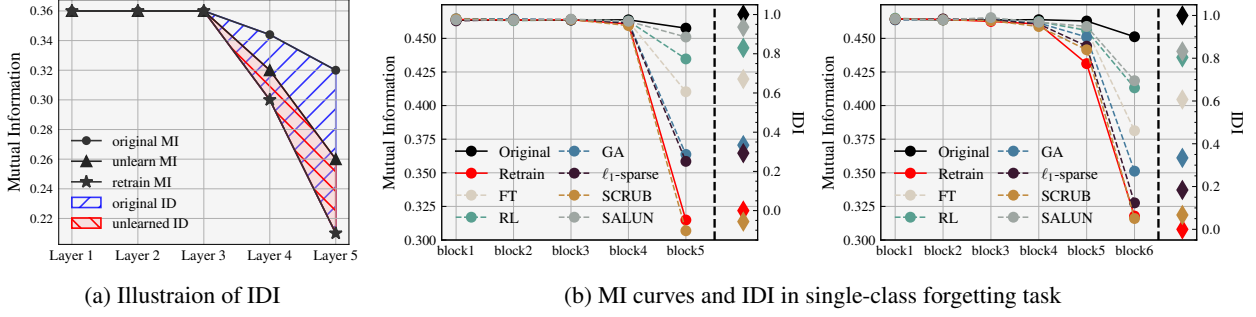


Figure 5: (a) Conceptual illustration of IDI. Curves show estimated mutual information $I(\mathbf{Z}_\ell; Y)$ for Original (\bullet), unlearned (\blacktriangle), and Retrain (\star). IDI is the ratio $\frac{ID(\theta_u)}{ID(\theta_o)}$, corresponding to the red area divided by the blue area. (b) MI curves and IDI values for Original, Retrain, and unlearned models from six methods (FT, RL, GA, ℓ_1 -sparse, SCRUB, SALUN) on CIFAR-10 across ResNet-18 (left) and ResNet-50 (right) blocks, averaged over five trials. See Appendix C.1 for standard deviations.

For f_{ν_ℓ} , we propose a model-agnostic approach that reuses the network layers from $\ell + 1$ to L , allowing us to approximate the mutual information between the output and intermediate features at layer ℓ without requiring network redesign for each layer, thus maintaining flexibility and scalability. To ensure dimensional compatibility between f and g , we introduce an additional linear projection layer so that $f_{\nu_\ell}(\mathbf{Z}_\ell)$ outputs a d -dimensional feature.

During the optimization of the InfoNCE loss, we freeze the parameters of the model up to the ℓ -th layer and reuse the architecture of the remaining layers, starting from $\ell + 1$, as f_{ν_ℓ} . These remaining layers, along with the projection layer, are randomly initialized and trained from scratch to specifically optimize the InfoNCE loss. We utilize both the retain set and the forget set to have representations for $Y = 0$ and $Y = 1$, ensuring that the model captures information relevant to both outcomes.

This approach allows f_{ν_ℓ} to effectively leverage intermediate features \mathbf{Z}_ℓ to classify Y , providing deeper insights into the model’s internal information processing at each layer. It also reveals the model’s capacity to extract and utilize relevant information for distinguishing between output labels, offering a clearer understanding of the information dynamics across the network.

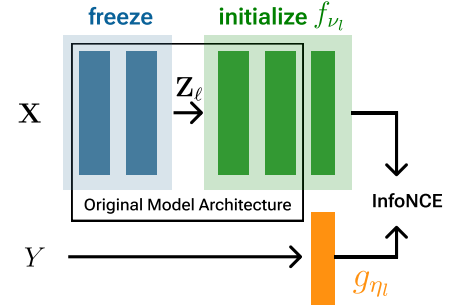


Figure 6: Illustration of estimating MI using InfoNCE. The critic function f_{ν_ℓ} represents a trainable network to capture features from \mathbf{Z}_ℓ , while the critic function g_{η_ℓ} handles the binary input Y .

4.2 Residual Information in Unlearned Models

We begin by plotting the estimated MI between the intermediate layers and the binary label indicating whether the data belong to the forget set, as shown in Figure 5b. As expected, MI decreases across layers, aligning with the Information Bottleneck principle [Tishby et al., 2000]. This figure reveals the internal behaviors of unlearned models that black-box assessments fail to capture.

In particular, SCRUB and ℓ_1 -sparse, which approximate the MI levels of Retrain, are more likely to achieve the MU objective at the feature level across both ResNet architectures. Their lower MI suggests that their encoders, like Retrain, struggle to differentiate between the forget set and the retain set. Conversely, SALUN and RL show MI curves that are close to that of Original, indicating the opposite. Note that HD produces the identical curve as Original, as its encoder remains unchanged. We observe similar patterns in CIFAR-100 and ImageNet-1K, as well as in ViT. Additionally, extending our experiment to multi-class forgetting tasks (e.g., 20 classes on CIFAR-100) reveals more pronounced MI differences between Retrain and Original. See Appendix D.1 for further results.

4.3 Information Difference Index (IDI)

Motivated from the above experiment, we define the **information difference (ID)** of θ_u as the MI difference across intermediate layers between the unlearned model and Retrain, calculated as:

$$\text{ID}(\theta_u) = \sum_{\ell=1}^L (I(\mathbf{Z}_\ell^{(u)}; Y) - I(\mathbf{Z}_\ell^{(r)}; Y)). \quad (1)$$

ID of θ_u shows the extent of information retention through ensuing layers of the unlearned encoder. To provide a normalized measure, we introduce the **information difference index (IDI)**:

$$\text{IDI}(\theta_u) = \frac{\text{ID}(\theta_u)}{\text{ID}(\theta_0)} = \frac{\sum_{\ell=1}^L (I(\mathbf{Z}_\ell^{(u)}; Y) - I(\mathbf{Z}_\ell^{(r)}; Y))}{\sum_{\ell=1}^L (I(\mathbf{Z}_\ell^{(o)}; Y) - I(\mathbf{Z}_\ell^{(r)}; Y))}, \quad (2)$$

where $\mathbf{Z}_\ell^{(o)}$ is the output of the ℓ -th layer of Original encoder. Figure 5a illustrates IDI, which is conceptually the ratio of the areas between MI curves.

IDI quantifies the information gap between the unlearned model and Retrain. An IDI of 0 denotes that the unlearned model has completely removed all information related to the forget set, achieving indistinguishability from Retrain. In contrast, an IDI of 1 indicates that the encoder retains all the information found in Original. Interestingly, a negative IDI value, termed *over-unlearning*, occurs when the model removes more information than Retrain. While we have demonstrated IDI in the context of class-wise forgetting, its application to random data forgetting is provided in Appendix A.1.

5 Experiments

5.1 Proposed Baseline: COLLapse and Align (COLA)

As discussed in both Section 3 and 4.2, we observed residual information in the intermediate layers of several unlearned models, despite their outputs being similar to those of Retrain. To address this, we propose a robust two-step unlearning framework, **COLLapse and Align (COLA)**, consisting of a *collapse phase* and an *alignment phase* to directly remove residual information at the feature level.

During the *collapse phase*, COLA eliminates feature-level information by applying supervised contrastive loss [Khosla et al., 2020] to encoder outputs. Rather than dispersing features from the forget set, which could harm model performance, COLA applies the loss to the retain set, promoting tight intra-class clustering. As these clusters shrink, features from the forget set are forced to collapse into the clusters of the retain set, achieving catastrophic forgetting. After feature collapsing, the *alignment phase* optimizes the entire model using cross-entropy loss on the retain set to align the encoder and head. For an illustration of COLA and a detailed loss formulation, refer to Appendix B.6.

5.2 Comprehensive Evaluation of Unlearning Methods with COLA and IDI

We demonstrate the utility of IDI as a valuable efficacy metric and highlight the strong performance of COLA through extensive experiments. Our experiments cover three datasets: CIFAR-10, CIFAR-100 [Krizhevsky, 2009], and ImageNet-1K [Deng et al., 2009], and three model architectures: ResNet-18, ResNet-50 [He et al., 2016], and ViT [Dosovitskiy et al., 2020]. For simplicity, we approximate IDI using the features from blocks rather than every layer in ResNet and ViT (see Appendix B.7). Please refer to Appendix B for further experimental details.

Table 1 shows the experimental results on CIFAR-10 and ImageNet-1K in class-forgetting tasks. At first glance, without the IDI column, several methods show similar accuracy (UA, RA, TA) but greater deviations in efficacy (MIA) and efficiency (RTE). This suggests that MIA and RTE likely determined the rankings of MU methods in previous unlearning studies. However, as discussed earlier, relying solely on black-box metrics can be misleading, as they fail to capture residual information. Indeed, some methods show strong efficacy on MIA yet fail to remove forget data from intermediate layers, as reflected by high IDI values. For instance, CF-5 on ImageNet-1K achieves a favorable MIA value (10.21) close to Retrain (9.41) in the shortest time (81.53 min), yet its IDI (0.701) shows significant retention of forget data. Similarly, EU-5, which appears highly efficient (1.54 min) on CIFAR-10, presents a high IDI (0.528), suggesting that its apparent efficiency may result from incomplete unlearning. By incorporating IDI alongside existing metrics, we gain a more comprehensive and insightful evaluation of MU methods.

Table 1: Performance summary of MU methods (including the proposed COLA and 11 other baselines) for class-wise forgetting task on (CIFAR-10, ResNet-18) and (ImageNet-1K, ResNet-50). The results are shown as $a \pm b$, with a being the mean and b the standard deviation of five independent trials. A better performance of an MU method corresponds to a smaller performance gap with Retrain (except RTE), with the top method in **bold** and the second best underlined.

Methods	CIFAR-10 (single class)						ImageNet-1K (five classes)					
	UA	RA	TA	MIA	IDI	RTE (min)	UA	RA	TA	MIA	IDI	RTE (min)
Retrain	100.0	100.0	95.64	10.64	0.0	154.56	100.0	88.80	75.88	9.41	0.0	2661.90
FT	100.0 $_{\pm 0.0}$	100.0 $_{\pm 0.0}$	95.12 $_{\pm 0.09}$	0.17 $_{\pm 0.05}$	0.671 $_{\pm 0.008}$	6.44 $_{\pm 0.07}$	100.0 $_{\pm 0.0}$	88.52 $_{\pm 0.0}$	<u>76.16</u> $_{\pm 0.01}$	8.24 $_{\pm 1.23}$	0.102 $_{\pm 0.026}$	140.04 $_{\pm 1.42}$
RL	99.93 $_{\pm 0.01}$	100.0 $_{\pm 0.0}$	95.66 $_{\pm 0.05}$	0.0 $_{\pm 0.0}$	0.830 $_{\pm 0.005}$	3.09 $_{\pm 0.03}$	<u>99.96</u> $_{\pm 0.03}$	86.46 $_{\pm 0.07}$	75.23 $_{\pm 0.01}$	0.23 $_{\pm 0.01}$	1.002 $_{\pm 0.007}$	200.73 $_{\pm 1.87}$
GA	100.0 $_{\pm 0.0}$	99.06 $_{\pm 0.25}$	93.10 $_{\pm 0.50}$	25.37 $_{\pm 3.24}$	0.334 $_{\pm 0.014}$	4.00 $_{\pm 0.08}$	100.0 $_{\pm 0.0}$	80.77 $_{\pm 0.22}$	71.49 $_{\pm 0.10}$	4.20 $_{\pm 0.46}$	0.328 $_{\pm 0.023}$	212.14 $_{\pm 2.61}$
Bad-T	99.90 $_{\pm 0.14}$	<u>99.99</u> $_{\pm 0.0}$	94.99 $_{\pm 0.12}$	68.17 $_{\pm 42.80}$	1.014 $_{\pm 0.004}$	4.64 $_{\pm 0.05}$	98.01 $_{\pm 0.02}$	84.03 $_{\pm 0.03}$	73.42 $_{\pm 0.03}$	69.13 $_{\pm 12.57}$	1.152 $_{\pm 0.011}$	211.52 $_{\pm 0.96}$
EU-5	100.0 $_{\pm 0.0}$	100.0 $_{\pm 0.0}$	95.25 $_{\pm 0.02}$	0.06 $_{\pm 0.03}$	0.528 $_{\pm 0.005}$	1.54 $_{\pm 0.0}$	100.0 $_{\pm 0.0}$	79.62 $_{\pm 0.0}$	71.22 $_{\pm 0.13}$	13.33 $_{\pm 1.53}$	0.183 $_{\pm 0.028}$	193.38 $_{\pm 0.78}$
CF-5	98.13 $_{\pm 1.39}$	100.0 $_{\pm 0.0}$	<u>95.54</u> $_{\pm 0.09}$	0.0 $_{\pm 0.0}$	0.675 $_{\pm 0.027}$	<u>1.57</u> $_{\pm 0.03}$	100.0 $_{\pm 0.0}$	84.31 $_{\pm 0.08}$	74.16 $_{\pm 0.06}$	10.21 $_{\pm 5.33}$	0.701 $_{\pm 0.014}$	81.53 $_{\pm 0.56}$
EU-10	100.0 $_{\pm 0.0}$	99.50 $_{\pm 0.02}$	93.61 $_{\pm 0.08}$	15.24 $_{\pm 1.08}$	-0.349 $_{\pm 0.019}$	2.42 $_{\pm 0.11}$	100.0 $_{\pm 0.0}$	71.84 $_{\pm 0.03}$	65.78 $_{\pm 0.02}$	16.65 $_{\pm 1.91}$	-0.051 $_{\pm 0.021}$	193.79 $_{\pm 0.47}$
CF-10	100.0 $_{\pm 0.0}$	99.98 $_{\pm 0.0}$	94.95 $_{\pm 0.05}$	11.61 $_{\pm 0.91}$	-0.060 $_{\pm 0.017}$	2.31 $_{\pm 0.03}$	100.0 $_{\pm 0.0}$	80.87 $_{\pm 0.04}$	72.34 $_{\pm 0.08}$	13.99 $_{\pm 5.41}$	0.608 $_{\pm 0.012}$	<u>82.29</u> $_{\pm 0.34}$
SCRUB	100.0 $_{\pm 0.0}$	100.0 $_{\pm 0.0}$	95.37 $_{\pm 0.04}$	19.73 $_{\pm 1.92}$	-0.056 $_{\pm 0.008}$	3.49 $_{\pm 0.02}$	99.28 $_{\pm 0.07}$	<u>88.39</u> $_{\pm 0.04}$	76.51 $_{\pm 0.03}$	7.42 $_{\pm 0.51}$	0.517 $_{\pm 0.011}$	426.04 $_{\pm 2.98}$
SALUN	<u>99.99</u> $_{\pm 0.01}$	100.0 $_{\pm 0.0}$	95.42 $_{\pm 0.12}$	0.01 $_{\pm 0.01}$	0.936 $_{\pm 0.012}$	3.54 $_{\pm 0.11}$	89.67 $_{\pm 0.27}$	86.25 $_{\pm 0.15}$	75.54 $_{\pm 0.10}$	0.50 $_{\pm 0.09}$	0.343 $_{\pm 0.017}$	793.82 $_{\pm 3.32}$
ℓ_1 -sparse	100.0 $_{\pm 0.0}$	99.93 $_{\pm 0.02}$	94.90 $_{\pm 0.10}$	1.56 $_{\pm 0.09}$	0.293 $_{\pm 0.012}$	2.90 $_{\pm 0.03}$	97.57 $_{\pm 0.61}$	85.33 $_{\pm 0.07}$	74.77 $_{\pm 0.03}$	<u>8.84</u> $_{\pm 1.39}$	0.239 $_{\pm 0.031}$	226.74 $_{\pm 1.35}$
COLA	100.0 $_{\pm 0.0}$	100.0 $_{\pm 0.0}$	95.36 $_{\pm 0.06}$	<u>12.64</u> $_{\pm 0.92}$	0.010 $_{\pm 0.006}$	4.91 $_{\pm 0.04}$	100.0 $_{\pm 0.0}$	87.93 $_{\pm 0.05}$	76.15 $_{\pm 0.04}$	9.95 $_{\pm 1.21}$	0.040 $_{\pm 0.042}$	171.44 $_{\pm 0.75}$

In Figure 7, we present the CIFAR-100 results comparing task performance (TA) and unlearning quality (IDI). Methods like Bad-T and RL achieve high accuracy but retain substantial residual information (high IDI). Conversely, EU-5 and ℓ_1 -sparse effectively remove forget set (low IDI) but suffer notable accuracy loss (low TA), indicating damage to essential features for task performance. Despite its simple design and without accessing the forget set, COLA consistently achieves state-of-the-art IDI performance across all experiments, as shown in Table 1 and Figure 7, effectively eliminating feature-level information. This capability is further supported by the previous experiment (see Figure 4), where COLA recovers low accuracy similar to Retrain. COLA also performs well on metrics like MIA and TA, preserving task performance and output similarity (see Table 1). While COLA’s computational cost (RTE) is relatively high, we emphasize that thoroughly removing forget set while maintaining model utility is challenging. Further experimental results for class-wise and random data forgetting are provided in Appendix C.

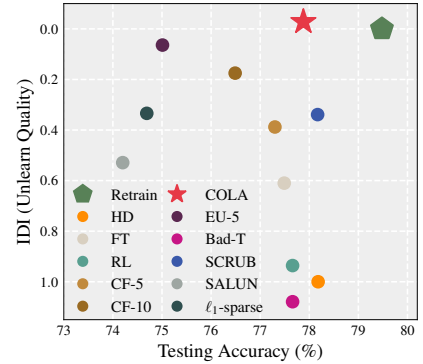


Figure 7: IDI and TA of Retrain and 11 MU methods in single-class forgetting (ResNet-18, CIFAR-100).

5.3 Discussions

Consistency and Scalability of IDI. Consistency is crucial for unlearning metrics, but many fall short [Chundawat et al., 2023a, Tarun et al., 2023b, Becker and Liebig, 2022]. Also, a major issue with using model parameters for white-box efficacy evaluation in DNNs is their inconsistency, as weights can vary significantly due to stochastic factors (e.g., random seeds), making comparisons between the unlearned model and Retrain ambiguous [Yang and Shami, 2020, Goel et al., 2022]. In contrast, IDI remains robust, delivering consistent results across models from the same algorithm, as evidenced by low standard deviations in independent trials (see Table 1).

Furthermore, IDI provides consistent results without requiring the entire dataset \mathcal{D} . As shown in Figure 8, the relative rankings of methods remain stable across different data ratios in the class-wise forgetting task on CIFAR-100. This efficiency allows for unlearning evaluations with reduced computational cost, where white-box metrics often demand significant resources.

IDI as a Real-World Efficacy Metric. Accuracy metrics (UA, RA, TA) and efficacy metrics (MIA, JSD), commonly used in recent unlearning studies, require the presence of Retrain as a gold standard to compare model outputs. While this approach is crucial for advancing MU methods in controlled experimental settings, where the field of unlearning for DNNs is still in its infancy, it becomes impractical in real-world applications where Retrain is unavailable. Similar to current black-box metrics, the original formulation of IDI (see Equations 1 and 2) uses Retrain as a reference to assess unlearning efficacy. However, IDI allows for flexibility by using any available unlearned model as the reference. Although the absence of

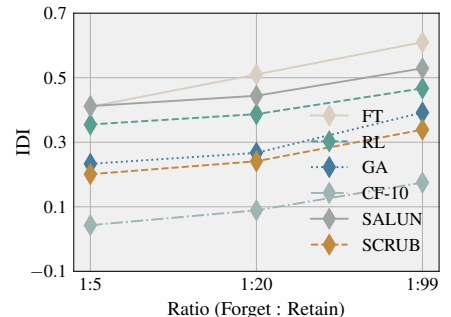


Figure 8: IDI of six methods with various binary label ratios, in the single-class forgetting task on (CIFAR-100, ResNet-18). The ratio $a : b$ indicates the relative amounts of forgetting and retaining samples, respectively.

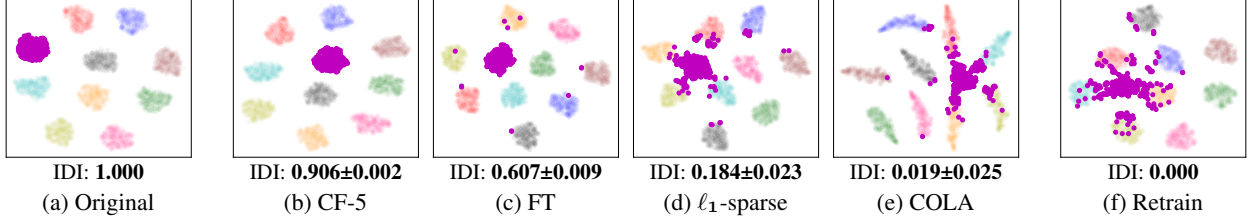


Figure 9: t-SNE visualizations of encoder outputs for Original, Retrain, and unlearned models from four MU methods (SALUN, ℓ_1 -sparse, SCRUB, EU-10) on single-class forgetting with (CIFAR-10, ResNet-50). In each t-SNE plot, features of the forgetting class are represented in purple.

Retrain changes the interpretation of IDI (*i.e.*, an IDI of zero means complete unlearning as Retrain), it still provides valuable insights relative to the chosen reference. This adaptability enhances the IDI’s practicality, making it useful for evaluating unlearned models even in real-world scenarios. A detailed explanation and examples are provided in Appendix D.2.

Correlation of IDI with t-SNE. In Section 3.2, we identified significant residual information in unlearned models through their tightly clustered t-SNE plots (see Figure 3) and their ability to easily recover forgotten information (see Figure 4). Black-box assessments failed to detect these residuals, as shown by the success of HD (see Figure 2), which only altered the last layer. In contrast, IDI effectively captures these hidden residuals, showing a strong correlation with t-SNE plots (see Figure 9), and aligning with accuracy recovered across unlearned models (see Figure 4). By complementing existing metrics, IDI offers a comprehensive evaluation of approximate MU methods, addressing crucial aspects to ensure strong unlearning beyond superficial modifications. Additional t-SNE results and their corresponding IDI values for various methods are available in Appendix D.3.

6 Conclusion

We highlight the limitations of relying on black-box metrics to assess unlearning efficacy in typical approximate unlearning studies. Although intermediate features capable of reconstructing forgotten information persist, these metrics fail to capture the key aspects required for strong unlearning, often misleading evaluations. To address this, we introduce the Information Difference Index (IDI) from an information-theoretic perspective, alongside the contrastive-based COLA baseline for direct feature-level unlearning. Through extensive experiments, we demonstrate the validity and practicality of IDI, showing that it complements existing metrics for a more comprehensive evaluation of strong unlearning. In addition, we highlight the effectiveness of the COLA baseline, despite its simplicity.

References

- N. Aldaghri, H. Mahdavifar, and A. Beirami. Coded machine unlearning. *IEEE Access*, 2021.
- A. Becker and T. Liebig. Evaluating machine unlearning via epistemic uncertainty. *arXiv preprint arXiv:2208.10836*, 2022.
- L. Bourtole, V. Chandrasekaran, C. A. Choquette-Choo, H. Jia, A. Travers, B. Zhang, D. Lie, and N. Papernot. Machine unlearning. In *ISSP*, 2021.
- J. Brophy and D. Lowd. Machine unlearning for random forests. In *ICML*, 2021.
- Y. Cao and J. Yang. Towards making systems forget with machine unlearning. In *ISSP*, 2015.
- N. Carlini, S. Chien, M. Nasr, S. Song, A. Terzis, and F. Tramer. Membership inference attacks from first principles. In *ISSP*, 2022.
- M. Chen, W. Gao, G. Liu, K. Peng, and C. Wang. Boundary unlearning: Rapid forgetting of deep networks via shifting the decision boundary. In *CVPR*, 2023.
- V. S. Chundawat, A. K. Tarun, M. Mandal, and M. Kankanhalli. Zero-shot machine unlearning. *IEEE Trans. Inf. Forensics Secur.*, 2023a.
- V. S. Chundawat, A. K. Tarun, M. Mandal, and M. Kankanhalli. Can bad teaching induce forgetting? unlearning in deep networks using an incompetent teacher. In *AAAI*, 2023b.
- G. Cohen and R. Giryès. Membership inference attack using self influence functions. In *WACV*, 2024.
- J. Deng, W. Dong, R. Socher, L.-J. Li, K. Li, and L. Fei-Fei. Imagenet: A large-scale hierarchical image database. In *CVPR*, 2009.
- A. Dosovitskiy, L. Beyer, A. Kolesnikov, D. Weissenborn, X. Zhai, T. Unterthiner, M. Dehghani, M. Minderer, G. Heigold, S. Gelly, et al. An image is worth 16x16 words: Transformers for image recognition at scale. *arXiv preprint arXiv:2010.11929*, 2020.
- C. Dwork and A. Roth. The algorithmic foundations of differential privacy. *Found. Trends Theor. Comput. Sci.*, 2014.
- C. Fan, J. Liu, Y. Zhang, D. Wei, E. Wong, and S. Liu. Salun: Empowering machine unlearning via gradient-based weight saliency in both image classification and generation. *arXiv preprint arXiv:2310.12508*, 2023.
- J. Foster, S. Schoepf, and A. Brintrup. Fast machine unlearning without retraining through selective synaptic dampening. In *AAAI*, 2024.
- R. M. French. Catastrophic forgetting in connectionist networks. *Trends Cogn Sci.*, 1999.
- A. Ginart, M. Guan, G. Valiant, and J. Y. Zou. Making ai forget you: Data deletion in machine learning. In *NeurIPS*, 2019.
- S. Goel, A. Prabhu, A. Sanyal, S.-N. Lim, P. Torr, and P. Kumaraguru. Towards adversarial evaluations for inexact machine unlearning. *arXiv preprint arXiv:2201.06640*, 2022.
- A. Gollatkar, A. Achille, and S. Soatto. Eternal sunshine of the spotless net: Selective forgetting in deep networks. In *CVPR*, 2020a.
- A. Gollatkar, A. Achille, and S. Soatto. Forgetting outside the box: Scrubbing deep networks of information accessible from input-output observations. In *ECCV*, 2020b.
- A. Gollatkar, A. Achille, A. Ravichandran, M. Polito, and S. Soatto. Mixed-privacy forgetting in deep networks. In *CVPR*, 2021.
- L. Graves, V. Nagisetty, and V. Ganesh. Amnesiac machine learning. In *AAAI*, 2021.
- C. Guo, T. Goldstein, A. Hannun, and L. Van Der Maaten. Certified data removal from machine learning models. *arXiv preprint arXiv:1911.03030*, 2019.
- J. Hayes, I. Shumailov, E. Triantafillou, A. Khalifa, and N. Papernot. Inexact unlearning needs more careful evaluations to avoid a false sense of privacy. *arXiv preprint arXiv:2403.01218*, 2024.
- K. He, X. Zhang, S. Ren, and J. Sun. Deep Residual Learning for Image Recognition. In *CVPR*, 2016.
- G. Hinton, O. Vinyals, and J. Dean. Distilling the knowledge in a neural network. *arXiv preprint arXiv:1503.02531*, 2015.
- C. Jia, Y. Yang, Y. Xia, Y.-T. Chen, Z. Parekh, H. Pham, Q. Le, Y.-H. Sung, Z. Li, and T. Duerig. Scaling up visual and vision-language representation learning with noisy text supervision. In *ICML*, 2021.

- P. Khosla, P. Teterwak, C. Wang, A. Sarna, Y. Tian, P. Isola, A. Maschinot, C. Liu, and D. Krishnan. Supervised contrastive learning. In *NeurIPS*, 2020.
- H. Kim, S. Lee, and S. S. Woo. Layer attack unlearning: Fast and accurate machine unlearning via layer level attack and knowledge distillation. In *AAAI*, 2024.
- P. Kirichenko, P. Izmailov, and A. G. Wilson. Last layer re-training is sufficient for robustness to spurious correlations. *ICLR*, 2023.
- J. Kirkpatrick, R. Pascanu, N. Rabinowitz, J. Veness, G. Desjardins, A. A. Rusu, K. Milan, J. Quan, T. Ramalho, A. Grabska-Barwinska, et al. Overcoming catastrophic forgetting in neural networks. *PNAS*, 2017.
- A. Krizhevsky. Learning multiple layers of features from tiny images. 2009.
- M. Kurmanji, P. Triantafillou, J. Hayes, and E. Triantafillou. Towards unbounded machine unlearning. In *NeurIPS*, 2024.
- J. Liu, P. Ram, Y. Yao, G. Liu, Y. Liu, P. SHARMA, S. Liu, et al. Model sparsity can simplify machine unlearning. In *NeurIPS*, 2024.
- S. Mu and D. Klabjan. Rewind-to-delete: Certified machine unlearning for nonconvex functions. *arXiv preprint arXiv:2409.09778*, 2024.
- M. Nasr, R. Shokri, and A. Houmansadr. Comprehensive privacy analysis of deep learning: Passive and active white-box inference attacks against centralized and federated learning. In *SP. IEEE*, 2019.
- S. Neel, A. Roth, and S. Sharifi-Malvajerdi. Descent-to-delete: Gradient-based methods for machine unlearning. In *ALT*, 2021.
- T. T. Nguyen, T. T. Huynh, P. L. Nguyen, A. W.-C. Liew, H. Yin, and Q. V. H. Nguyen. A survey of machine unlearning. *arXiv preprint arXiv:2209.02299*, 2022.
- A. v. d. Oord, Y. Li, and O. Vinyals. Representation learning with contrastive predictive coding. *arXiv preprint arXiv:1807.03748*, 2018.
- B. Poole, S. Ozair, A. Van Den Oord, A. Alemi, and G. Tucker. On variational bounds of mutual information. In *ICML*, 2019.
- X. Qiao, M. Zhang, M. Tang, and E. Wei. Efficient online unlearning via hessian-free recollection of individual data statistics. *arXiv preprint arXiv:2404.01712*, 2024.
- A. Radford, J. W. Kim, C. Hallacy, A. Ramesh, G. Goh, S. Agarwal, G. Sastry, A. Askell, P. Mishkin, J. Clark, et al. Learning transferable visual models from natural language supervision. In *ICML*, 2021.
- R. Rombach, A. Blattmann, D. Lorenz, P. Esser, and B. Ommer. High-resolution image synthesis with latent diffusion models. In *CVPR*, 2022.
- A. Sekhari, J. Acharya, G. Kamath, and A. T. Suresh. Remember what you want to forget: Algorithms for machine unlearning. *NeurIPS*, 2021.
- T. Shaik, X. Tao, H. Xie, L. Li, X. Zhu, and Q. Li. Exploring the landscape of machine unlearning: A survey and taxonomy. *arXiv preprint arXiv:2305.06360*, 2023.
- C. E. Shannon. A mathematical theory of communication. *The Bell System Technical Journal*, 1948.
- S. Shen, C. Zhang, Y. Zhao, A. Bialkowski, W. T. Chen, and M. Xu. Label-agnostic forgetting: A supervision-free unlearning in deep models. In *ICLR*, 2023.
- R. Shokri, M. Stronati, C. Song, and V. Shmatikov. Membership inference attacks against machine learning models. In *ISSP*, 2017.
- A. K. Tarun, V. S. Chundawat, M. Mandal, and M. Kankanhalli. Deep regression unlearning. In *ICML*, 2023a.
- A. K. Tarun, V. S. Chundawat, M. Mandal, and M. Kankanhalli. Fast yet effective machine unlearning. *IEEE Trans. Neural Netw. Learn. Syst.*, 2023b.
- A. Thudi, G. Deza, V. Chandrasekaran, and N. Papernot. Unrolling sgd: Understanding factors influencing machine unlearning. In *EuroS&P*, 2022.
- N. Tishby and N. Zaslavsky. Deep learning and the information bottleneck principle. In *ITW*, 2015.
- N. Tishby, F. C. Pereira, and W. Bialek. The information bottleneck method. *arXiv preprint physics/0004057*, 2000.
- H. Touvron, T. Lavril, G. Izacard, X. Martinet, M.-A. Lachaux, T. Lacroix, B. Rozière, N. Goyal, E. Hambro, F. Azhar, et al. Llama: Open and efficient foundation language models. *arXiv preprint arXiv:2302.13971*, 2023.
- E. Ullah, T. Mai, A. Rao, R. A. Rossi, and R. Arora. Machine unlearning via algorithmic stability. In *COLT*, 2021.

- L. van der Maaten and G. Hinton. Visualizing data using t-sne. *JMLR*, 2008.
- P. Voigt and A. Von dem Bussche. The eu general data protection regulation (gdpr). *Springer International Publishing*, 2017.
- Y. Wu, E. Dobriban, and S. Davidson. Deltagrad: Rapid retraining of machine learning models. In *ICML*, 2020.
- H. Xu, T. Zhu, L. Zhang, W. Zhou, and P. Yu. Machine unlearning: A survey. *ACM Computing Surveys*, 2023.
- H. Yan, X. Li, Z. Guo, H. Li, F. Li, and X. Lin. Arcane: An efficient architecture for exact machine unlearning. In *IJCAI*, 2022.
- L. Yang and A. Shami. On hyperparameter optimization of machine learning algorithms: Theory and practice. *Neurocomputing*, 2020.
- B. Zhang, Y. Dong, T. Wang, and J. Li. Towards certified unlearning for deep neural networks. *arXiv preprint arXiv:2408.00920*, 2024.

A Random Data Forgetting

Another scenario in machine unlearning (MU) is *random data forgetting*, which involves forgetting a randomly selected subset of data across multiple classes. This differs from the *class-wise forgetting* task, which aims to forget entire data from single or multiple classes.

A.1 Information Difference Index for Random Data Forgetting

To calculate the information difference index (IDI) for class-wise forgetting, we employ a binary label Y to determine whether a sample belongs to the retain or forget set. However, this approach is inadequate for random data forgetting, where samples span multiple classes and a minor fraction of each class is targeted for forgetting. As a result, no single class is completely removed. To address this, we transform the binary label Y into a multiclass label Y_C , which reflects the ground-truth class label of each sample. Consequently, we define the IDI for random data forgetting as follows:

$$\text{IDI}_{\text{random}}(\theta_{\mathbf{u}}) = \frac{\text{ID}_{\text{random}}(\theta_{\mathbf{u}})}{\text{ID}_{\text{random}}(\theta_0)}, \quad (3)$$

where $\text{ID}_{\text{random}}(\theta_{\mathbf{u}}) = \sum_{\ell=1}^L (I(\mathbf{Z}_{\ell}^{(\mathbf{u})}; Y_C) - I(\mathbf{Z}_{\ell}^{(\mathbf{r})}; Y_C))$. Unlike the ID computed in a class-wise forgetting, $\text{ID}_{\text{random}}(\cdot)$ utilizes only the forget set \mathcal{D}_f . Intuitively, we expect the mutual information $I(\mathbf{Z}^{(\mathbf{o})}; Y_C)$ to be higher than $I(\mathbf{Z}^{(\mathbf{r})}; Y_C)$ because Original explicitly learned the relationship between the forget samples and their ground truth labels, while Retrain did not. Although the labels have transitioned from binary to multiple classes, the function $f_{\nu_{\ell}}$ remains unchanged. For $g_{\eta_{\ell}}$, it now employs the C dimension of vectors, where C represents the total number of data classes.

A.2 COLA+

The core idea behind COLA is to induce catastrophic forgetting within the model’s encoder in the collapse phase, making the influence of the forget set vanish implicitly. This approach is effective for class-wise forgetting tasks, where the forget set includes distinct classes. However, it may be less effective for random data forgetting, where the forget set and retain set samples generally share the same classes and are not easily distinguishable. To address this, we aim to explicitly remove the information of the forget set through pseudo-labeling. This variant, called COLA+, assigns the second-highest predicted label to the forget set samples before unlearning with supervised contrastive loss [Khosla et al., 2020]. This pseudo-labeling effectively collapsing the forget set features into the retain set clusters of other classes, while reducing the confusion of the knowledge of the retain set. The results of the COLA+ experiment on the random data forgetting task are presented in Appendix C.4.

B Experiment Details

B.1 Evaluation Metrics Detail

UA, RA, TA We compute accuracy as follows:

$$\text{Acc}_{\mathcal{D}}(\theta) = \frac{1}{|\mathcal{D}|} \sum_{(x,y) \in \mathcal{D}} \mathbb{1}[\arg \max(f(x; \theta)) = y], \quad (4)$$

where $f(x; \theta)$ represents the model’s output logits for input x with parameters θ , and y is the ground truth label. Unlearning accuracy (UA), which quantifies the model’s task performance on forgetting data, is defined as $UA(\theta_{\mathbf{u}}) = 1 - \text{Acc}_{\mathcal{D}_f}(\theta_{\mathbf{u}})$. Remaining accuracy (RA) measures the model’s performance on the retain set \mathcal{D}_r , which should be preserved after unlearning, and is defined as $RA(\theta_{\mathbf{u}}) = \text{Acc}_{\mathcal{D}_r}(\theta_{\mathbf{u}})$. Finally, testing accuracy (TA) evaluates generalization to unseen data, and is defined as $TA(\theta_{\mathbf{u}}) = \text{Acc}_{\mathcal{D}_{\text{test}}}(\theta_{\mathbf{u}})$. It is important to note that better unlearning in terms of accuracy reflects a smaller performance gap between the unlearned model and Retrain, meaning that higher accuracy levels are not necessarily better. Refer to [Liu et al., 2024] for detailed explanation.

MIA. Membership Inference Attack (MIA) [Shokri et al., 2017, Carlini et al., 2022] determines whether a specific data record was part of a model’s training set by leveraging auxiliary classifiers to distinguish between training and non-training data based on the model’s output.

In the context of unlearning, membership inference attack (MIA) is primarily used as an evaluation metric, rather than representing an adversarial scenario where an attacker attempts to extract membership information from the unlearned

model. Consequently, a comparable MIA success rate on the forgetting data relative to Retrain signifies a more effective unlearning algorithm. Unlike the original MIA implementation [Shokri et al., 2017], which utilizes multiple shadow models, MIA variants in the unlearning often employ a single auxiliary classifier for each unlearning method [Liu et al., 2024]. A detailed comparison of these approaches can be found in [Hayes et al., 2024].

The MIA implementation in our study has two phases: the *training phase* and the *testing phase*.

During the *training phase*, we create a balanced dataset by equally sampling from the retain set (\mathcal{D}_r) and the test set, explicitly excluding the forget set (\mathcal{D}_f). We then use this balanced dataset to train the MIA predictor with two output categories (train, non-train), allowing it to differentiate between training and non-training samples.

In the *testing phase*, the trained MIA predictor is used to evaluate the efficacy of the unlearning methods. Specifically, the **MIA** metric is calculated by applying the MIA predictor to the unlearned model (θ_u) using the forget set (\mathcal{D}_f). The objective is to determine how many samples within \mathcal{D}_f are identified as training samples by the MIA predictor.

Formally, MIA is defined as:

$$\text{MIA} = 1 - \frac{\text{TN}}{|\mathcal{D}_f|} \quad (5)$$

where TN represents the number of true negatives (*i.e.*, the number of forget samples correctly predicted as non-training examples by the MIA predictor), and $|\mathcal{D}_f|$ denotes the total number of samples in the forget set. Overall, MIA leverages privacy attack mechanisms to validate the effectiveness of the unlearning process, providing a quantitative measure of how successfully the model has ‘forgotten’ specific data resembling Retrain.

We consider two widely adopted variants of MIA. The first variant, **C-MIA (Confidence-based MIA)**, assesses membership based on the confidence score, which is the predicted probability of the true class [Kurmanji et al., 2024, Liu et al., 2024]. The second variant, **E-MIA (Entropy-based MIA)**, infers membership by examining the entropy of the model’s outputs, calculated as $H(x) = -\sum_i \mathbf{p}_i(x) \cdot \log \mathbf{p}_i(x)$ [Chundawat et al., 2023b, Foster et al., 2024]. Higher entropy indicates greater uncertainty in the model’s predictions, often signaling non-training samples. We primarily report results using E-MIA due to its more pronounced differences across various baselines compared to C-MIA. It is noteworthy that our head distillation (HD) method achieves similar performance outcomes with both E-MIA and C-MIA.

JSD Jensen-Shannon divergence (JSD) is presented in Bad-T [Chundawat et al., 2023b]. It measures the distance between the output distributions of the unlearned model and Retrain. JSD is measured as follows:

$$\text{JSD}_{\mathcal{D}}(\theta_u, \theta_r) = 0.5 \cdot KL(f(x; \theta_u) \parallel m) + 0.5 \cdot KL(f(x; \theta_r) \parallel m), \quad (6)$$

where $KL(\cdot)$ is Kullback-Leibler divergence, x is data from \mathcal{D} , and $m = \frac{f(x; \theta_u) + f(x; \theta_r)}{2}$. Here, $f(x; \theta)$ represents the model’s output probability distribution for input x with parameters θ . A smaller distance means better unlearning as the unlearned model better mimics Retrain.

RTE Runtime efficiency (RTE) measures the time that an algorithm spends to complete the unlearning, where smaller RTE indicates more efficient unlearning [Fan et al., 2023, Liu et al., 2024, Foster et al., 2024]. Since it measures the experiment wall-clock time, it has high variance depending on the experiment environment.

B.2 Approximate MU Baselines.

We conduct our experiments on several widely used or recent approximate MU baselines: Finetuning (**FT**) [Golatkari et al., 2020a] finetunes Original θ_o with retain set \mathcal{D}_r , inducing catastrophic forgetting [French, 1999, Kirkpatrick et al., 2017] of \mathcal{D}_f . Random labeling (**RL**) [Golatkari et al., 2020a] involves finetuning θ_o with randomly labeled forget set \mathcal{D}_f . Gradient ascent (**GA**) [Thudi et al., 2022] trains θ_o with reverse gradient steps using \mathcal{D}_f . **Bad-T** [Chundawat et al., 2023b] uses a teacher-student framework that utilizes distillation techniques, distinguishing between beneficial and detrimental influences through good and bad teachers to refine the learning process. Catastrophic forgetting-k (**CF-k**) and exact unlearning-k (**EU-k**) [Goel et al., 2022] involve either finetuning (CF-k) or retraining (EU-k) the last k layers of the model using \mathcal{D}_r while freezing the prior layers. **SCRUB** [Kurmanji et al., 2024] employs a technique of positive distillation from θ_o using the \mathcal{D}_r , and negative distillation on the \mathcal{D}_f , which helps in selectively retaining beneficial knowledge while discarding the unwanted influences. ℓ_1 -**sparse** [Liu et al., 2024] enhances the model’s ability to forget by strategically inducing weight sparsity in θ_o . **SALUN** [Fan et al., 2023] finetunes the salient weights of θ_o using a method that incorporates random labeling.

Table 2: Training configuration for Original and Retrain.

Settings	CIFAR-10 / CIFAR-100		ImageNet-1K	
	Resnet-18 / Resnet-50	ViT	ResNet-50	ViT
Epochs	300	3	90	30
Batch Size	128		256	512
LR	0.1	0.00002	0.1	0.02
Optimizer	SGD			
Momentum	0.9			
L2 regularization	0.0005		0	
Scheduler	CosineAnnealing			

B.3 Datasets and Models

We conduct image classification experiments utilizing well-established datasets and models. The datasets include CIFAR-10, CIFAR-100 [Krizhevsky, 2009], and ImageNet-1K [Deng et al., 2009]; and the models are ResNet-18, ResNet-50 [He et al., 2016], and Vision Transformer (ViT) [Dosovitskiy et al., 2020]. CIFAR-10 and CIFAR-100 each comprise 50,000 training images distributed across 10 and 100 classes, respectively, each with an original resolution of 32 x 32 pixels. In our experiments, we resize the images in ImageNet-1K, which consists of 1,281,167 training images across 1,000 classes, to 224 x 224 pixels. Similarly, for the ViT experiments, we resize CIFAR images to 224 x 224 pixels to accommodate the architecture’s requirements. Throughout the training process, including pretraining and unlearning phases, we employ basic data augmentation techniques such as random cropping and random horizontal flipping.

B.4 Pretraining Settings

To perform unlearning, we require two models: **Original**, trained on the entire dataset \mathcal{D} , and **Retrain**, trained on the retain set \mathcal{D}_r . Original initializes the unlearning model. After unlearning, Retrain evaluates them. Table 2 summarizes the training configurations for each dataset and model combination. We train ResNet models from scratch and initialize ViT models with ImageNet-21K pretrained weights. For training on ImageNet-1K, we follow the configurations provided by Pytorch³.

B.5 Unlearning Settings

We aim to follow the hyperparameters provided by the original papers. However, many hyperparameters are missing since most existing works do not experiment with large-scale datasets and models. Additionally, some values from the original papers result in poor performance, likely due to different experiment settings, as most previous work performed unlearning without any data augmentation, unlike our experiments. Therefore, we conduct thorough hyperparameter searches for each baseline. The detailed hyperparameters of each baseline, including our method COLA and COLA+, are shown in Table 5 and Table 6. We use the same optimizer and batch size from the original papers and focus on finding the best epoch number and learning rate in terms of unlearning accuracy (UA) and testing accuracy (TA). Note that we implement gradient ascent (GA) from SCRUB [Kurmanji et al., 2024] (referred to as ‘NegGrad+’) due to its strong performance.

B.6 COLA and COLA+ Pseudo Code

Algorithm 1 shows the pseudo code of our two-step framework COLA. Only using the retain set \mathcal{D}_r , in the *collapse phase* (see Figure 10), We first train the encoder of the model using supervised contrastive loss [Khosla et al., 2020] as follows:

$$\text{SupConLoss}(b, \theta_{\text{enc}}) = \frac{1}{|b|} \sum_i \frac{1}{|P(i)|} \sum_{p \in P(i)} -\log \frac{\exp(\mathbf{z}_i \cdot \mathbf{z}_p / \tau)}{\sum_{a \in A(i)} \exp(\mathbf{z}_i \cdot \mathbf{z}_a / \tau)}, \quad (7)$$

³<https://github.com/pytorch/examples/tree/main/imagenet>

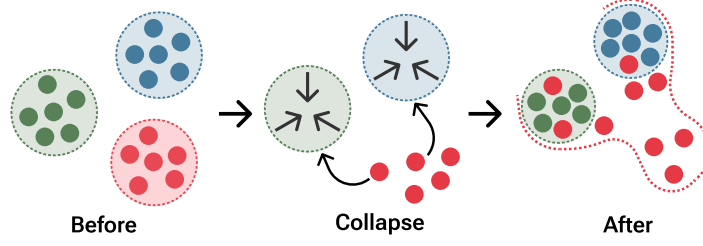


Figure 10: Illustration of the collapse phase of COLA. Features (post-encoder, pre-head) from forget set \mathcal{D}_f are represented in red, while features from retain set \mathcal{D}_r are represented in green and blue. The figure shows a class-wise forgetting task. Best viewed in color.

where $P(i)$ is the set of indices of positive samples sharing the same label as sample i , $A(i)$ is the set of all indices excluding sample i , τ is a temperature, and $z_i = F(x_i; \theta_{\text{enc}})$, the output feature of the model encoder. Then we train the whole network using cross-entropy loss in the *align phase*. COLA+ additionally utilizes forget set \mathcal{D}_f in the collapse phase, where the label of forget samples is changed to the class label closest to the original label, determined by the logit output of the head of Original. Its pseudo code is presented in Algorithm 2.

Algorithm 1 Pseudo Code of COLA

Require: learning rate η , number of epochs E_1, E_2 , retain set $\mathcal{D}_r = \{(x_i, y_i) \mid (x_i, y_i) \in \mathcal{D}_r\}$, encoder $F(\cdot; \theta)$, and model weight $\theta = \{\theta_{\text{enc}}, \theta_{\text{head}}\}$

```

 $\theta_{\text{u,enc}} \leftarrow \theta_{\text{o,enc}}$  ▷ Collapse phase
for  $e \leftarrow 0$  to  $E_1 - 1$  do
    for all batches  $b$  of  $\mathcal{D}_r$  do
         $L = \text{SupConLoss}(b, \theta_{\text{u,enc}})$  ▷ Equation 7
         $\theta_{\text{u,enc}} \leftarrow \theta_{\text{u,enc}} - \eta \nabla_{\theta_{\text{u,enc}}} L$ 
    end for
end for

 $\theta_{\text{u,head}} \leftarrow \text{random initialization}$  ▷ Align phase
for  $e \leftarrow 0$  to  $E_2 - 1$  do
    for all batches  $b$  of  $\mathcal{D}_r$  do
         $\theta_{\text{u}} \leftarrow \theta_{\text{u}} - \eta \nabla_{\theta_{\text{u}}} L_{CE}$ 
    end for
end for
return  $\theta_{\text{u}} = \{\theta_{\text{u,enc}}, \theta_{\text{u,head}}\}$ 
    
```

B.7 IDI Details

To derive IDI from features, it is necessary to train the critic functions f_{ν_ℓ} and g_{η_ℓ} , as referenced in Section 4. For the training of g_{η_ℓ} , a learning rate of $5 \cdot 10^{-4}$ is applied in all architectures and datasets. Meanwhile, for f_{ν_ℓ} , the learning rates are set at $2 \cdot 10^{-5}$ for CIFAR10 ResNet-18, $2 \cdot 10^{-6}$ for ViT ImageNet-1K, and $1 \cdot 10^{-5}$ for the remaining architectures of the data set.

To get IDI, we analyzed the outputs from the layers of different models. Specifically, we evaluated the last two bottleneck outputs for ResNet18 and the final three for ResNet50. For Vision Transformer (ViT), we examined the outputs of the final three transformer encoder blocks. Note that these selections of layers is based on the observation that the information differences of outputs from the initial layers of both original and retrained models are similar.

B.8 System specification

For fair comparison, all experiments are executed in Python 3.10, on an Ubuntu 18.04 machine with 72 CPU cores, 4 Nvidia RTX A6000 GPUs and 512GB memory.

Algorithm 2 Pseudo Code of COLA+

Require: learning rate η , number of epochs E_1, E_2 , retain set $\mathcal{D}_r = \{(x_i, y_i) \mid (x_i, y_i) \in \mathcal{D}_r\}$, forget set $\mathcal{D}_f = \{(x'_i, y'_i) \mid (x'_i, y'_i) \in \mathcal{D}_f\}$, encoder $F(\cdot; \theta)$, head $G(\cdot; \theta)$, and model weight $\theta = \{\theta_{\text{enc}}, \theta_{\text{head}}\}$

$\theta_{\text{u,enc}} \leftarrow \theta_{\text{o,enc}}$ ▷ Collapse phase
 $\theta_{\text{u,head}} \leftarrow \theta_{\text{o,head}}$
for $e \leftarrow 0$ **to** $E_1 - 1$ **do**
 for $\{b_r, b_f\}$ in all batches of $\{\mathcal{D}_r, \mathcal{D}_f\}$ **do**
 for $x'_i \in b_f$ **do**
 $y'_i \leftarrow \arg \max_y \text{softmax}(G(F(x'_i; \theta_{\text{u,enc}}); \theta_{\text{u,head}})) \cdot \mathbb{I}[y \neq y'_i]$ ▷ Pseudo-labeling
 end for
 $b \leftarrow b_r + b_f$
 $L = \text{SupConLoss}(b, \theta_{\text{u,enc}})$ ▷ Equation 7
 $\theta_{\text{u,enc}} \leftarrow \theta_{\text{u,enc}} - \eta \nabla_{\theta_{\text{u,enc}}} L$
 end for
end for ▷ Align phase

for $e \leftarrow 0$ **to** $E_2 - 1$ **do**
 for all batches b of \mathcal{D}_r **do**
 $\theta_{\text{u}} \leftarrow \theta_{\text{u}} - \eta \nabla_{\theta_{\text{u}}} L_{CE}$
 end for
end for
return $\theta_{\text{u}} = \{\theta_{\text{u,enc}}, \theta_{\text{u,head}}\}$

C Additional Unlearning Results

In this section, we provide the full experiment results on various machine unlearning settings, extending the results in Section 4 and Section 5.2.

C.1 Standard Deviation

Due to the visual complexity of Figures 5 and 8, representing the standard deviation directly in these figures is challenging. Therefore, we include the standard deviation values separately in Tables 12 and 13 for Figure 5, and in Table 14 for Figure 8.

C.2 Single-Class Forgetting Results

CIFAR-10 with Various Architectures Table 7 shows the full experiment results of the single-class forgetting experiments from Table 1 on CIFAR-10 using different models. This extended table includes Jensen-Shannon divergence (JSD) and the unlearning results with ResNet-50 and ViT. Although many baselines show promising results on output based evaluation metrics, they generally exhibit poor feature-level unlearning. In contrast, COLA not only outperforms existing baselines in IDI but also shows decent results in other metrics, demonstrating its effectiveness in removing the influence of the forget set within the encoder of the model.

CIFAR-100 with Various Architectures As demonstrated in Table 8, we also compare COLA with other baselines on CIFAR-100. The results consistently highlight the difficulty of comparing and validating the efficacy of each unlearning method using existing output-based metrics. With the help of IDI, it is clear that COLA shows robustness in model unlearning on datasets with a large number of classes across various model architectures. Although SCRUB has achieved IDI near 0 for the CIFAR-10 ResNet-18 experiment, it shows significant variations in feature-level unlearning across different datasets and architectures.

C.3 Multi-Class Forgetting Results

Multi-Class Forgetting on CIFAR-10 and CIFAR-100 Table 9 presents the results of multi-class forgetting experiments on CIFAR-10 and CIFAR-100 using ResNet-18, which involves erasing the information of more than one class in the training set. We remove two classes from CIFAR-10 and five and twenty classes from CIFAR-100. Notably, many baselines exhibit higher IDI values as the number of forgetting class increases, demonstrating that the

tendency to modify the head of the model strengthens with the difficulty of the unlearning tasks. In contrast, COLA shows remarkable effectiveness, achieving metric values closely aligned with Retrain. Specifically, COLA consistently achieves the lowest IDI values among the evaluated methods, indicating the necessity of the collapse phase for effective feature-level unlearning no matter the number of class to forget.

Multi-Class Forgetting on ImageNet-1K We conduct 5-class unlearning on ImageNet-1K using ResNet-50 and ViT. Table 10 provides the complete results of Table 1 for ImageNet-1K, including all evaluation metrics and outcomes on the ViT architecture. However, it is important to note that IDI alone should not be used to assess unlearned models, as a low IDI might indicate a loss of overall information, including that from the retain set, which should be maintained at the same level as Original. This issue is evident in the RA, TA, and IDI of EU-10 and CF-10 in Table 10. In contrast, COLA consistently achieves IDI near 0 while maintaining accuracy measurements comparable to Retrain, demonstrating the scalability of our framework to the large-scale datasets.

C.4 Random Data Forgetting Results

Table 11 presents the results of the random data forgetting task conducted on ResNet-18. For CIFAR-10 and CIFAR-100 datasets, we randomly selected 500 and 50 forget samples per class, respectively. COLA+, which incorporates pseudo-labeling, successfully eliminates the influence of the forgetting data while maintaining competitive performance.

D Additional Discussions

D.1 Mutual Information Curves

Figure 14 illustrates the estimated mutual information $I(\mathbf{Z}_\ell; Y)$ of the features from the ℓ -th layer \mathbf{Z}_ℓ and the binary label Y , computed by the InfoNCE loss across various architectures and datasets. We compute mutual information (MI) for all layers from the ResNet encoder and last five layers from the ViT encoder based single-class forgetting retain and forget sets. The upper bound of MI is given by the entropy $H(Y) \geq I(\mathbf{Z}_\ell; Y) = H(Y) - H(Y | \mathbf{Z}_\ell)$. The estimated MI values fall within the range of the upper and lower bounds (0), validating the use of InfoNCE for MI estimation. Notably, all MI curves consistently show a larger difference between Original and Retrain in the later layers of the encoder across various datasets and architectures, while differences are minimal in the earlier layers. These observations underscore the validity of computing the information difference (ID) for the last few layers to quantify unlearning. Furthermore, the difference between Original and Retrain becomes more significant with increasing numbers of forget classes, as shown in Figure 15.

D.2 IDI without Retrain Model

In real-world applications, using the Retrain is often infeasible. In such cases, any reasonable model can be used as the **standard model**, denoted as θ_s . Although the absence of a Retrain inevitably affects how the IDI value is interpreted (*i.e.*, an IDI value of zero indicates that unlearning has been properly achieved, equivalent to the Retrain), it still provides useful insights into the degree of unlearning achieved relative to the chosen reference. To accommodate this, we introduce an extended version of the ID metric. Differences are highlighted with (\cdot) :

$$\text{ID}(\theta_u, \theta_s) = \sum_{\ell=1}^L \left(I(\mathbf{Z}_\ell^{(u)}; Y_C) - I(\mathbf{Z}_\ell^{(s)}; Y_C) \right). \quad (8)$$

The main difference from the original ID is that θ_s can be set as any model including θ_r (Retrain), while the previous version fixed $\theta_s = \theta_r$. This extension also leads to the modified IDI metric:

$$\text{IDI}(\theta_u, \theta_s) = \frac{\text{ID}(\theta_u, \theta_s)}{\text{ID}(\theta_o, \theta_s)} = \frac{\sum_{\ell=1}^L \left(I(\mathbf{Z}_\ell^{(u)}; Y) - I(\mathbf{Z}_\ell^{(s)}; Y) \right)}{\sum_{\ell=1}^L \left(I(\mathbf{Z}_\ell^{(o)}; Y) - I(\mathbf{Z}_\ell^{(s)}; Y) \right)}. \quad (9)$$

We test IDI using different reference models, as demonstrated in Table 3. Intuitively, since only the standard model changes in Equation (9), the order of the IDI values remains consistent.

D.3 IDI and t-SNE Relationship

Figure 11 presents t-SNE plots illustrating the intermediate features and corresponding IDI measurements of MU baselines on the single-class unlearning on CIFAR-10 with ResNet-18. In the plots, the purple points represent the

Table 3: IDI for four different reference models (Retrain, COLA, EU-10, and FT*). FT* is finetuned with a learning rate of $5e-5$, while FT is finetuned with a learning rate of $1e-5$. Since FT typically does not remove all residual information while maintaining test accuracy, using a higher learning rate for FT* can be justified if you want to use it as the reference model. The ‘Order’ has been arranged in ascending sequence according to the IDI values.

Methods	CIFAR-10					CIFAR-100				
	Order	θ_s = Retrain	θ_s = COLA	θ_s = EU-10	θ_s = FT*	Order	θ_s = Retrain	θ_s = COLA	θ_s = EU-10	θ_s = FT*
FT	8	$0.671_{\pm 0.008}$	$0.668_{\pm 0.008}$	$0.756_{\pm 0.006}$	$0.662_{\pm 0.008}$	11	$0.610_{\pm 0.022}$	$0.624_{\pm 0.021}$	$0.680_{\pm 0.018}$	$0.481_{\pm 0.029}$
RL	10	$0.830_{\pm 0.005}$	$0.828_{\pm 0.005}$	$0.874_{\pm 0.004}$	$0.825_{\pm 0.005}$	9	$0.467_{\pm 0.010}$	$0.486_{\pm 0.010}$	$0.563_{\pm 0.008}$	$0.291_{\pm 0.013}$
GA	6	$0.334_{\pm 0.014}$	$0.328_{\pm 0.014}$	$0.506_{\pm 0.010}$	$0.315_{\pm 0.014}$	8	$0.392_{\pm 0.021}$	$0.414_{\pm 0.020}$	$0.502_{\pm 0.017}$	$0.191_{\pm 0.028}$
Bad-T	12	$1.014_{\pm 0.004}$	$1.014_{\pm 0.004}$	$1.010_{\pm 0.003}$	$1.014_{\pm 0.004}$	12	$1.079_{\pm 0.024}$	$1.076_{\pm 0.023}$	$1.065_{\pm 0.020}$	$1.105_{\pm 0.032}$
EU-5	7	$0.528_{\pm 0.005}$	$0.523_{\pm 0.005}$	$0.650_{\pm 0.004}$	$0.515_{\pm 0.005}$	3	$0.064_{\pm 0.037}$	$0.098_{\pm 0.036}$	$0.233_{\pm 0.030}$	$-0.245_{\pm 0.049}$
CF-5	9	$0.675_{\pm 0.027}$	$0.672_{\pm 0.027}$	$0.759_{\pm 0.020}$	$0.666_{\pm 0.028}$	7	$0.388_{\pm 0.010}$	$0.410_{\pm 0.010}$	$0.499_{\pm 0.008}$	$0.186_{\pm 0.013}$
EU-10	1	$-0.349_{\pm 0.019}$	$-0.362_{\pm 0.019}$	$0.0_{\pm 0.014}$	$-0.387_{\pm 0.020}$	1	$-0.221_{\pm 0.009}$	$-0.177_{\pm 0.009}$	$0.0_{\pm 0.007}$	$-0.624_{\pm 0.012}$
CF-10	2	$-0.060_{\pm 0.017}$	$-0.070_{\pm 0.017}$	$0.214_{\pm 0.013}$	$-0.090_{\pm 0.017}$	4	$0.175_{\pm 0.040}$	$0.205_{\pm 0.039}$	$0.324_{\pm 0.033}$	$-0.097_{\pm 0.053}$
SCRUB	3	$-0.056_{\pm 0.008}$	$-0.066_{\pm 0.008}$	$0.217_{\pm 0.006}$	$-0.086_{\pm 0.008}$	6	$0.339_{\pm 0.069}$	$0.363_{\pm 0.067}$	$0.458_{\pm 0.057}$	$0.121_{\pm 0.092}$
SALUN	11	$0.936_{\pm 0.012}$	$0.935_{\pm 0.012}$	$0.953_{\pm 0.009}$	$0.934_{\pm 0.012}$	10	$0.529_{\pm 0.022}$	$0.546_{\pm 0.021}$	$0.614_{\pm 0.018}$	$0.373_{\pm 0.029}$
ℓ_1 -sparse	5	$0.293_{\pm 0.012}$	$0.286_{\pm 0.012}$	$0.476_{\pm 0.009}$	$0.273_{\pm 0.012}$	5	$0.334_{\pm 0.026}$	$0.358_{\pm 0.025}$	$0.454_{\pm 0.021}$	$0.114_{\pm 0.035}$
COLA	4	$0.010_{\pm 0.006}$	$0.0_{\pm 0.006}$	$0.266_{\pm 0.004}$	$-0.018_{\pm 0.006}$	2	$-0.038_{\pm 0.006}$	$0.0_{\pm 0.006}$	$0.150_{\pm 0.005}$	$-0.381_{\pm 0.008}$

forgetting class. A high IDI corresponds to better clustering and similarity among features of the forgetting class, as seen in (l) SALUN and (f) Bad-T, which show inadequate unlearning performance. These examinations show the high relationship between IDI and the residual information of forget set. Additionally, the IDI metric reveals instances of over-unlearning, where the forgetting class becomes excessively dispersed, as demonstrated in (i) EU-10. Among the evaluated methods, (n) COLA has the closest IDI to Retrain, suggesting its high efficacy in achieving the desired removal of the forget set influence in the intermediate layers of the model. This trend is also visible in ResNet-50 (see Figure 12) and ViT (see Figure 13).

Furthermore, we confirm that IDI for the random data forgetting correctly captures the encoder’s information, similar to IDI for the class-wise forgetting. In Figure 17, the t-SNE plots of forget sample features for two baselines with the same unlearning accuracy (UA) – Bad-T and ℓ_1 -sparse – and their IDI values in the random data forgetting task is visualized. Comparing them, IDI successfully reflects the residual information in the features, as the features of Bad-T form more compact clusters than those of ℓ_1 -sparse, indicating more influence of the forget set remains in Bad-T. IDI the for random data forgetting captures the hidden information that cannot be noticed from existing metrics, which may suggest that both methods unlearn similarly due to their same forget accuracy.

D.4 Mutual Information and Accuracy

We extend the experiment to measure the accuracy of the intermediate features of the model’s encoder. Similar to measuring MI using the InfoNCE loss, we freeze the layers up to the ℓ -th layer of the encoder and train the remaining encoder layers and an additional head using cross-entropy loss. The additional head perform binary classification to determine whether the input belongs to the retain or forget set.

Figure 16 shows the train accuracy curves on the CIFAR-10 single-class forgetting dataset with ResNet-18. For Original encoder, the trained model readily classifies the retain and forget sets. However, for Retrain encoder, the model fails to classifies all samples at the last two layers, with the accuracy dropping more in the later layer. These curves correspond to the those from Figure 14, indicating that the estimated MI accurately reflects the model’s knowledge of the retain and forget sets. In addition, the small accuracy gap between Original and Retrain provides the necessity of MI for accurate residual information quantification.

D.5 Comparison of IDI with White-Box MIA

To examine whether current white MIA metrics in other research area can be directly applied for unlearning research, we implement well-known and recent white-box MIA [Nasr et al., 2019, Cohen and Giryas, 2024]. Table 4 show that training an attack model with activations or gradient norms produces a behavior similar to our IDI metric on the CIFAR10 dataset, with a lower attack success rate as the information of forget samples decreases. However, these methods lack stability as the dataset size increases (*i.e.*, CIFAR100), resulting in noisy and hard-to-analyze results. For the experience, we transform the white box MIA into the unlearning form of MIA.

To validate our metric, we compare the performance of white-box MIAs and IDI using a randomly initialized model (Method “Initialized” in Table 4), which is expected to have no information on the forget set. IDI shows values of -1.281 for CIFAR10 and -2.955 for CIFAR100 with low standard deviation, indicating significantly less information than the Retrain model, which is desirable. In contrast, white-box MIAs produce noisy results with a high standard

Table 4: Performance of unlearning algorithms on white-box MIAs (Activation, Gradient, Influence) and IDI. The values of white-box MIAs is the success rate (%) of distinguishing the forget samples. “Initialized” is for the model randomly initialized.

Methods	CIFAR-10				CIFAR-100			
	Activation	Gradient	Influence	IDI	Activation	Gradient	Influence	IDI
Original	99.98 \pm 0.03	100.0 \pm 0.0	93.0 \pm 0.07	1.000	53.13 \pm 2.88	61.34 \pm 3.23	99.3 \pm 0.10	1.000
Retrain	94.89 \pm 1.07	95.13 \pm 1.12	0.0 \pm 0.0	0.000	52.87 \pm 6.15	59.12 \pm 4.12	0.0 \pm 0.0	0.000
Initialized	52.89 \pm 41.03	45.23 \pm 23.04	17.0 \pm 4.32	-1.281 \pm 0.018	53.20 \pm 5.15	47.12 \pm 7.21	13.0 \pm 3.75	-2.955 \pm 0.046
RL	100.0 \pm 0.0	99.98 \pm 0.01	0.0 \pm 0.0	0.830 \pm 0.005	93.20 \pm 3.53	95.30 \pm 0.82	0.40 \pm 0.02	0.467 \pm 0.010
GA	97.07 \pm 0.35	96.01 \pm 0.13	0.0 \pm 0.0	0.334 \pm 0.014	97.44 \pm 2.12	82.44 \pm 0.95	0.0 \pm 0.0	0.392 \pm 0.021
EU-10	86.13 \pm 4.78	89.42 \pm 2.32	0.0 \pm 0.0	-0.349 \pm 0.019	64.41 \pm 1.65	72.13 \pm 4.13	0.0 \pm 0.0	-0.221 \pm 0.009
CF-10	97.99 \pm 0.38	98.33 \pm 0.23	0.0 \pm 0.0	-0.060 \pm 0.017	21.62 \pm 0.61	23.15 \pm 1.23	0.0 \pm 0.0	0.175 \pm 0.040
SCRUB	99.43 \pm 0.09	99.15 \pm 0.05	0.0 \pm 0.0	-0.056 \pm 0.008	46.44 \pm 1.28	62.31 \pm 1.73	0.0 \pm 0.0	0.339 \pm 0.069
COLA	92.26 \pm 0.08	93.12 \pm 0.11	0.0 \pm 0.0	0.010 \pm 0.006	61.08 \pm 0.23	65.24 \pm 0.43	0.0 \pm 0.0	-0.038 \pm 0.006

deviation, making them difficult to interpret. Although some variations of white-box MIAs might work as a stable metric, we believe it is nontrivial to devise one as a rigorous metric for MU. We also consider IDI to be interpreted as a form of white-box MIA, which could be an interesting direction for future research.

E Broader Impact

Our work on improving machine unlearning focuses on foundational research aimed at enhancing privacy and data removal. However, there is a potential risk that our methodology could be misused to evade data retention policies or obscure accountability. Despite this possibility, it is unlikely that our work will introduce new harmful practices beyond what existing unlearning methods already permit, as we are not introducing new capabilities. Therefore, while there might be concerns related to privacy, security, and fairness, our work does not pose a greater risk compared to other foundational research in machine unlearning.

F Limitations

Our methodology accomplishes its main objective, but there are a few limitations we point out. Although our IDI successfully investigates hidden information in intermediate features, its computation requires multiple training runs, which can be computationally intensive. For instance, The computation of IDI for ResNet-50 on the CIFAR-100 dataset takes approximately 40-50 minutes. However, one can mitigate this by computing mutual information for only the last few layers, as the early stages of the encoder are largely similar for both the Retrain and Original models. Thus, this approach requires fine-tuning only the later layers, reducing the overall computational burden. Additionally, by adjusting the forget-to-retain ratio, it is possible to improve efficiency and possibly decrease the processing time to merely 3-4 minutes.

Table 5: Hyperparameters of baselines for *class-wise forgetting*. Retain Batch Size is the batch size of retain set \mathcal{D}_r and Forget Batch Size is the batch size of forget set \mathcal{D}_f . Baselines without Forget Batch Size imply that they do not use forget set \mathcal{D}_f . Bad-T uses the entire dataset \mathcal{D} , so there is no separation of retain and forget of Batch Size. SCRUB has separate epochs for retain set and forget set, which is visualized as Retain Epochs (Forget Epochs). For COLA, A + B Epochs indicates collapse epochs A and align epochs B.

Class-wise Forgetting			
Settings	CIFAR-10 ResNet-18 / ResNet-50 / ViT	CIFAR-100 ResNet-18 / ResNet-50 / ViT	ImageNet-1K ResNet-50 / ViT
FT	25 Epochs, Adam LR $10^{-5}/10^{-5}/10^{-4}$ Retain Batch Size 64		3/4 Epochs, Adam LR 10^{-5} Retain Batch Size 128
RL	7 / 7 / 10 Epochs, SGD LR $10^{-5} / 2 \cdot 10^{-5} / 10^{-3}$ Retain Batch Size 64 Forget Batch Size 16	7 / 7 / 10 Epochs, SGD LR $2 \cdot 10^{-5} / 10^{-4} / 10^{-4}$ Retain Batch Size 64 Forget Batch Size 16	3 Epochs, SGD LR $10^{-3} / 10^{-4}$ Retain Batch Size 128 Forget Batch Size 16
GA	10 Epochs, SGD LR $2 \cdot 10^{-3} / 2 \cdot 10^{-3} / 5 \cdot 10^{-3}$ Retain Batch Size 64 Forget Batch Size 16	10 Epochs, SGD LR $9 \cdot 10^{-4} / 9 \cdot 10^{-4} / 5 \cdot 10^{-3}$ Retain Batch Size 64 Forget Batch Size 16	3 Epochs, SGD LR $2 \cdot 10^{-3} / 10^{-3}$ Retain Batch Size 128 Forget Batch Size 16
Bad-T	10 Epochs, Adam LR 10^{-5} Batch Size 256		3 Epochs, Adam LR 10^{-5} Batch Size 256
EU-5 / EU-10	14 Epochs, SGD LR 10^{-2} Retain Batch Size 64		5 Epochs, SGD LR $5 \cdot 10^{-3}$ Retain Batch Size 128
CF-5 / CF-10	14 / 14 / 18 Epochs, SGD LR $10^{-2} / 10^{-2} / 3 \cdot 10^{-2}$ Retain Batch Size 64		2 Epochs, SGD LR $5 \cdot 10^{-3}$ Retain Batch Size 128
SCRUB	3(2) Epochs, SGD LR $5 \cdot 10^{-4} / 5 \cdot 10^{-4} / 10^{-4}$ Retain Batch Size 64 Forget Batch Size 256 / 256 / 64	3(2) Epochs, SGD LR $5 \cdot 10^{-4}$ Retain Batch Size 128 Forget Batch Size 8	2(2) Epochs, SGD LR $5 \cdot 10^{-4} / 10^{-4}$ Retain Batch Size 128 Forget Batch Size 256
SALUN	10 Epochs, SGD LR $5 \cdot 10^{-4} / 10^{-3} / 10^{-3}$ Retain Batch Size 64 Forget Batch Size 16	15 Epochs, SGD LR 10^{-3} Retain Batch Size 64 Forget Batch Size 16	5/2 Epochs, SGD LR 10^{-3} Retain Batch Size 128 Forget Batch Size 16
ℓ_1 -sparse	10 Epochs, SGD LR $2 \cdot 10^{-4} / 2 \cdot 10^{-4} / 9 \cdot 10^{-4}$ Retain Batch Size 64	10 Epochs, SGD LR $2 \cdot 10^{-4} / 2 \cdot 10^{-4} / 5 \cdot 10^{-4}$ Retain Batch Size 64	5 Epochs, SGD LR $9 \cdot 10^{-4}$ Retain Batch Size 128
COLA	10+10 Epochs, Adam Contrast LR $2 \cdot 10^{-4} / 2 \cdot 10^{-4} / 1.5 \cdot 10^{-4}$ Finetune LR $5 \cdot 10^{-6} / 10^{-5} / 5 \cdot 10^{-5}$ Retain Batch Size 64	10+10 Epochs, Adam Contrast LR $5 \cdot 10^{-4} / 5 \cdot 10^{-4} / 5 \cdot 10^{-4}$ Finetune LR $5 \cdot 10^{-6} / 10^{-5} / 5 \cdot 10^{-5}$ Retain Batch Size 256	1+2 Epochs, Adam Contrast LR $2 \cdot 10^{-5} / 5 \cdot 10^{-5}$ Finetune LR $1 \cdot 10^{-5} / 5 \cdot 10^{-5}$ Retain Batch Size 256

Table 6: Hyperparameters of baselines for *random data forgetting*. Retain Batch Size is the batch size of retain set \mathcal{D}_r and Forget Batch Size is the batch size of forget set \mathcal{D}_f . Baselines without Forget Batch Size imply that they do not use forget set \mathcal{D}_f . Bad-T uses the entire dataset \mathcal{D} , so there is no separation of retain and forget of Batch Size. SCRUB uses separate epochs for retain set and forget set, which is visualized as Retain Epochs (Forget Epochs). For COLA+, A + B Epochs indicates collapse epochs A and align epochs B.

Random Data Forgetting		
Settings	CIFAR-10 ResNet-18	CIFAR-100
FT	25 Epochs, Adam LR 10^{-4} Retain Batch Size 64	LR $2 \cdot 10^{-4}$
RL	7 Epochs, SGD LR 10^{-3} Retain Batch Size 64 Forget Batch Size 16	LR $5 \cdot 10^{-4}$
GA	10 Epochs, SGD LR $2.5 \cdot 10^{-3}$ Retain Batch Size 64 Forget Batch Size 16	10 Epochs, SGD LR $1 \cdot 10^{-3}$
Bad-T	10 Epochs, Adam LR $1 \cdot 10^{-5}$ Batch Size 256	
EU-5 / EU-10	14 Epochs, SGD LR 10^{-1} Retain Batch Size 64	LR $5 \cdot 10^{-2}$
CF-5 / CF-10	14 Epochs, SGD LR 10^{-1} Retain Batch Size 64	LR $5 \cdot 10^{-2}$
SCRUB	5(5) Epochs, SGD LR $2.5 \cdot 10^{-5}$ Retain Batch Size 16 Forget Batch Size 64	LR $5.4 \cdot 10^{-4}$
SALUN	10 Epochs, SGD LR $8.3 \cdot 10^{-4}$ Retain Batch Size 64 Forget Batch Size 16	15 Epochs, SGD LR $5 \cdot 10^{-4}$
ℓ_1 -sparse	10 Epochs, SGD LR $4 \cdot 10^{-4}$ Retain Batch Size 64	LR $3 \cdot 10^{-4}$ Retain Batch Size 64
COLA+	10+10 Epochs, Adam Contrast LR $2 \cdot 10^{-4}$ Finetune LR $1 \cdot 10^{-4}$ Retain Batch Size 32 Forget Batch Size 64	10+10 Epochs, Adam Contrast LR $2.5 \cdot 10^{-4}$ Finetune LR $2 \cdot 10^{-5}$ Retain Batch Size 64 Forget Batch Size 192

Table 7: Single-class forgetting result on CIFAR-10 dataset across different model architectures. A better performance of an MU method corresponds to a smaller performance gap with Retrain (except RTE), with the top method in **bold** and the second best underlined. The \star symbol indicated in RTE of Original and Retrain means that models are pretrained on ImageNet-21K and then finetuned on CIFAR-10, with the reported time reflecting only the finetuning process. In contrast, Original and Retrain without \star are trained from scratch on CIFAR-10.

CIFAR-10 - ResNet-18							
Methods	UA	RA	TA	MIA	JSD	IDI	RTE (min)
Original	0.0	100.0	95.46	91.50	3.21	1.000	170.32
Retrain	100.0	100.0	95.64	10.64	0.0	0.0	154.56
FT	100.0 ± 0.0	100.0 ± 0.0	95.12 ± 0.09	0.17 ± 0.05	0.57 ± 0.03	0.671 ± 0.008	6.44 ± 0.07
RL	99.93 ± 0.01	100.0 ± 0.0	95.66 ± 0.09	0.0 ± 0.0	0.79 ± 0.01	0.830 ± 0.005	3.09 ± 0.03
GA	100.0 ± 0.0	99.06 ± 0.25	93.10 ± 0.50	25.37 ± 3.24	0.59 ± 0.05	0.334 ± 0.014	4.00 ± 0.08
Bad-T	99.90 ± 0.14	<u>99.99</u> ± 0.0	94.99 ± 0.12	68.17 ± 42.80	3.69 ± 0.85	1.014 ± 0.004	4.64 ± 0.05
EU-5	100.0 ± 0.0	100.0 ± 0.0	95.25 ± 0.02	0.06 ± 0.03	0.53 ± 0.02	0.528 ± 0.005	1.54 ± 0.00
CF-5	98.13 ± 1.39	100.0 ± 0.0	<u>95.54</u> ± 0.09	0.0 ± 0.0	0.56 ± 0.04	0.675 ± 0.027	<u>1.57</u> ± 0.03
EU-10	100.0 ± 0.0	99.50 ± 0.02	<u>93.61</u> ± 0.08	15.24 ± 1.08	0.40 ± 0.01	-0.349 ± 0.019	2.42 ± 0.11
CF-10	100.0 ± 0.0	99.98 ± 0.0	94.95 ± 0.05	11.61 ± 0.91	<u>0.41</u> ± 0.01	-0.060 ± 0.017	2.31 ± 0.03
SCRUB	100.0 ± 0.0	100.0 ± 0.0	95.37 ± 0.04	19.73 ± 1.92	0.47 ± 0.01	<u>-0.056</u> ± 0.008	3.49 ± 0.02
SALUN	<u>99.99</u> ± 0.01	100.0 ± 0.0	95.42 ± 0.12	0.01 ± 0.01	0.73 ± 0.04	0.936 ± 0.012	3.54 ± 0.11
ℓ_1 -sparse	100.0 ± 0.0	99.93 ± 0.02	94.90 ± 0.10	1.56 ± 0.09	0.47 ± 0.03	0.293 ± 0.012	2.96 ± 0.03
COLA	100.0 ± 0.0	100.0 ± 0.00	95.36 ± 0.06	<u>12.64</u> ± 0.92	0.44 ± 0.04	0.010 ± 0.006	4.91 ± 0.04
CIFAR-10 - ResNet-50							
Methods	UA	RA	TA	MIA	JSD	IDI	RTE (min)
Original	0.0	100.0	95.42	95.58	4.11	1.000	341.86
Retrain	100.0	100.0	95.49	14.92	0.0	0.0	312.24
FT	100.0 ± 0.0	<u>99.99</u> ± 0.0	95.28 ± 0.11	2.17 ± 1.28	0.73 ± 0.02	0.607 ± 0.009	14.50 ± 0.34
RL	100.0 ± 0.0	100.0 ± 0.0	95.56 ± 0.03	0.0 ± 0.0	0.99 ± 0.02	0.804 ± 0.006	6.26 ± 0.04
GA	100.0 ± 0.0	98.06 ± 0.34	92.07 ± 0.63	20.56 ± 3.87	0.66 ± 0.06	0.334 ± 0.023	8.69 ± 0.03
Bad-T	100.0 ± 0.0	99.94 ± 0.04	94.74 ± 0.24	49.95 ± 40.74	3.02 ± 0.64	1.153 ± 0.026	10.19 ± 0.32
EU-5	100.0 ± 0.0	100.0 ± 0.0	95.59 ± 0.08	0.0 ± 0.0	0.78 ± 0.08	1.047 ± 0.005	<u>4.86</u> ± 0.43
CF-5	<u>17.84</u> ± 0.93	100.0 ± 0.0	95.64 ± 0.11	0.0 ± 0.0	1.43 ± 0.04	0.906 ± 0.002	4.84 ± 0.10
EU-10	100.0 ± 0.0	100.0 ± 0.0	<u>95.51</u> ± 0.12	0.17 ± 0.05	0.65 ± 0.02	0.757 ± 0.011	6.92 ± 0.02
CF-10	100.0 ± 0.0	100.0 ± 0.0	95.49 ± 0.13	0.07 ± 0.03	0.67 ± 0.08	0.579 ± 0.009	7.09 ± 0.02
SCRUB	100.0 ± 0.0	100.0 ± 0.0	95.23 ± 0.20	<u>18.19</u> ± 0.10	0.59 ± 0.01	<u>0.067</u> ± 0.020	8.69 ± 0.03
SALUN	100.0 ± 0.0	99.67 ± 0.17	93.90 ± 0.48	1.58 ± 0.98	0.67 ± 0.03	0.832 ± 0.027	11.00 ± 0.06
ℓ_1 -sparse	100.0 ± 0.0	99.88 ± 0.06	94.49 ± 0.29	4.06 ± 0.91	0.47 ± 0.01	0.184 ± 0.023	12.33 ± 0.04
COLA	100.0 ± 0.0	<u>99.99</u> ± 0.0	95.45 ± 0.05	13.69 ± 0.84	<u>0.52</u> ± 0.02	0.019 ± 0.025	11.98 ± 0.03
CIFAR-10 - ViT							
Methods	UA	RA	TA	MIA	JSD	IDI	RTE (min)
Original	0.36	99.55	98.40	89.12	3.96	1.000	100.68 \star
Retrain	100.0	99.40	97.96	4.96	0.0	0.0	90.96 \star
FT	98.10 ± 0.24	99.85 ± 0.06	97.58 ± 0.36	21.14 ± 0.92	0.71 ± 0.13	-0.871 ± 0.141	130.13 ± 0.63
RL	97.88 ± 2.12	99.88 ± 0.01	99.01 ± 0.02	0.0 ± 0.0	0.74 ± 0.04	1.052 ± 0.011	65.45 ± 0.12
GA	100.0 ± 0.0	99.80 ± 0.03	98.49 ± 0.12	4.82 ± 0.98	0.39 ± 0.05	0.498 ± 0.025	68.32 ± 0.80
Bad-T	100.0 ± 0.0	99.55 ± 0.03	<u>98.40</u> ± 0.20	0.0 ± 0.0	0.84 ± 0.06	0.997 ± 0.016	100.90 ± 1.02
EU-5	100.0 ± 0.0	99.76 ± 0.01	98.80 ± 0.01	0.30 ± 0.01	0.28 ± 0.03	0.901 ± 0.006	<u>29.89</u> ± 0.09
CF-5	100.0 ± 0.0	99.76 ± 0.0	98.86 ± 0.02	0.35 ± 0.03	0.26 ± 0.01	0.941 ± 0.001	34.12 ± 0.09
EU-10	100.0 ± 0.0	99.72 ± 0.02	98.63 ± 0.04	0.64 ± 0.02	<u>0.23</u> ± 0.03	<u>0.268</u> ± 0.016	32.74 ± 0.19
CF-10	100.0 ± 0.0	99.77 ± 0.01	98.75 ± 0.02	0.64 ± 0.04	0.21 ± 0.02	0.377 ± 0.039	36.79 ± 0.15
SCRUB	100.0 ± 0.0	<u>99.66</u> ± 0.0	98.57 ± 0.01	94.74 ± 0.26	3.87 ± 0.07	0.907 ± 0.027	22.99 ± 0.24
SALUN	100.0 ± 0.0	99.78 ± 0.02	98.89 ± 0.02	0.01 ± 0.01	0.39 ± 0.05	1.066 ± 0.041	61.37 ± 0.10
ℓ_1 -sparse	100.0 ± 0.0	97.48 ± 0.27	95.78 ± 0.16	<u>3.89</u> ± 0.79	0.41 ± 0.03	-0.573 ± 0.290	51.44 ± 0.04
COLA	<u>99.44</u> ± 0.02	100.0 ± 0.0	98.82 ± 0.06	11.90 ± 1.36	0.63 ± 0.11	-0.067 ± 0.010	116.01 ± 0.96

Table 8: Single-class forgetting result on CIFAR-100 dataset across different model architectures. A better performance of an MU method corresponds to a smaller performance gap with Retrain (except RTE), with the top method in **bold** and the second best underlined. The * symbol indicated in RTE of Original and Retrain means that models are pretrained on ImageNet-21K and then finetuned on CIFAR-100, with the reported time reflecting only the finetuning process. In contrast, Original and Retrain without are * trained from scratch on CIFAR-100.

CIFAR-100 - ResNet-18							
Methods	UA	RA	TA	MIA	JSD	IDI	RTE (min)
Original	0.0	99.98	78.18	92.80	2.91	1.000	175.08
Retrain	100.0	99.96	79.48	2.00	0.0	0.0	171.27
FT	100.0 ± 0.0	99.97 ± 0.0	77.49 ± 0.14	0.07 ± 0.09	0.37 ± 0.01	0.610 ± 0.022	9.50 ± 0.03
RL	93.80 ± 0.75	<u>99.98</u> ± 0.0	<u>77.94</u> ± 0.10	0.0 ± 0.0	0.52 ± 0.01	0.467 ± 0.010	3.52 ± 0.0
GA	<u>99.93</u> ± 0.09	<u>96.87</u> ± 0.52	69.87 ± 0.78	21.40 ± 2.04	1.18 ± 0.02	0.392 ± 0.021	5.32 ± 0.01
Bad-T	100.0 ± 0.0	<u>99.98</u> ± 0.0	77.66 ± 0.26	40.87 ± 36.87	2.53 ± 0.44	1.079 ± 0.024	5.78 ± 0.02
EU-5	100.0 ± 0.0	99.78 ± 0.01	75.01 ± 0.04	9.33 ± 0.75	0.66 ± 0.01	<u>0.064</u> ± 0.037	2.14 ± 0.0
CF-5	100.0 ± 0.0	99.97 ± 0.0	77.30 ± 0.28	2.87 ± 0.66	0.40 ± 0.03	0.388 ± 0.010	2.14 ± 0.01
EU-10	100.0 ± 0.0	91.94 ± 0.08	72.84 ± 0.04	12.67 ± 0.47	0.53 ± 0.02	-0.221 ± 0.009	4.39 ± 0.02
CF-10	100.0 ± 0.0	99.89 ± 0.02	76.49 ± 0.02	7.07 ± 0.84	0.49 ± 0.01	0.175 ± 0.040	4.29 ± 0.04
SCRUB	100.0 ± 0.0	<u>99.98</u> ± 0.0	78.17 ± 0.04	0.07 ± 0.09	<u>0.31</u> ± 0.01	0.339 ± 0.069	<u>2.27</u> ± 0.02
SALUN	95.73 ± 0.85	99.22 ± 0.13	74.20 ± 0.52	<u>0.09</u> ± 0.02	0.65 ± 0.01	0.529 ± 0.022	4.63 ± 0.06
ℓ_1 -sparse	96.93 ± 0.19	98.90 ± 0.12	74.69 ± 0.06	6.60 ± 0.43	0.34 ± 0.01	0.334 ± 0.026	4.55 ± 0.01
COLA	100.0 ± 0.0	99.80 ± 0.00	76.48 ± 0.11	9.60 ± 1.31	0.26 ± 0.01	-0.037 ± 0.006	7.51 ± 0.02
CIFAR-100 - ResNet-50							
Methods	UA	RA	TA	MIA	JSD	IDI	RTE (min)
Original	0.0	99.98	79.84	91.60	3.43	1.000	345.54
Retrain	100.0	99.97	79.42	3.40	0.0	0.0	338.58
FT	99.33 ± 0.09	99.93 ± 0.03	77.71 ± 0.18	0.40 ± 0.16	0.57 ± 0.02	0.618 ± 0.018	16.34 ± 0.47
RL	100.0 ± 0.0	99.95 ± 0.02	<u>79.56</u> ± 0.04	0.0 ± 0.0	0.80 ± 0.0	0.649 ± 0.013	8.38 ± 0.14
GA	99.60 ± 0.43	98.00 ± 0.72	<u>72.73</u> ± 1.16	13.33 ± 4.43	0.99 ± 0.04	0.526 ± 0.009	9.50 ± 0.54
Bad-T	100.0 ± 0.0	99.90 ± 0.10	77.53 ± 1.21	94.80 ± 2.75	3.98 ± 0.25	0.990 ± 0.033	12.69 ± 1.54
EU-5	100.0 ± 0.0	99.97 ± 0.01	78.31 ± 0.21	<u>1.20</u> ± 0.99	0.61 ± 0.04	0.520 ± 0.023	<u>6.81</u> ± 0.01
CF-5	100.0 ± 0.0	99.97 ± 0.01	78.98 ± 0.16	0.27 ± 0.09	0.50 ± 0.02	0.575 ± 0.016	6.82 ± 0.01
EU-10	100.0 ± 0.0	98.52 ± 0.14	75.66 ± 0.03	15.00 ± 1.45	0.69 ± 0.01	<u>0.050</u> ± 0.004	7.81 ± 0.01
CF-10	100.0 ± 0.0	99.95 ± 0.01	78.47 ± 0.10	5.87 ± 0.09	0.50 ± 0.02	0.302 ± 0.035	7.82 ± 0.02
SCRUB	100.0 ± 0.0	99.97 ± 0.0	79.61 ± 0.09	0.20 ± 0.16	<u>0.43</u> ± 0.02	0.620 ± 0.034	4.59 ± 0.13
SALUN	99.73 ± 0.38	<u>99.98</u> ± 0.0	79.51 ± 0.15	0.0 ± 0.0	0.80 ± 0.01	0.679 ± 0.010	12.83 ± 0.87
ℓ_1 -sparse	96.20 ± 0.16	99.42 ± 0.06	76.16 ± 0.31	2.60 ± 0.33	<u>0.43</u> ± 0.01	0.325 ± 0.018	15.78 ± 0.05
COLA	100.0 ± 0.0	99.90 ± 0.01	78.59 ± 0.28	10.27 ± 0.90	0.42 ± 0.02	0.016 ± 0.031	16.25 ± 0.10
CIFAR-100 - ViT							
Methods	UA	RA	TA	MIA	JSD	IDI	RTE (min)
Original	7.00	95.85	90.78	69.20	2.71	1.000	102.45*
Retrain	100.0	95.79	90.58	10.00	0.0	0.0	94.29*
FT	100.0 ± 0.0	99.79 ± 0.04	88.69 ± 0.11	14.80 ± 2.40	0.57 ± 0.03	-0.934 ± 0.011	140.61 ± 0.25
RL	99.19 ± 0.23	97.11 ± 0.02	92.28 ± 0.06	0.31 ± 0.01	0.82 ± 0.01	1.091 ± 0.031	73.12 ± 0.18
GA	100.0 ± 0.0	98.19 ± 0.20	90.59 ± 0.21	17.60 ± 4.78	0.31 ± 0.01	0.587 ± 0.011	75.22 ± 0.61
Bad-T	95.80 ± 0.08	95.88 ± 0.12	90.15 ± 0.02	0.0 ± 0.0	1.11 ± 0.14	1.213 ± 0.002	96.43 ± 0.01
EU-5	100.0 ± 0.0	97.59 ± 0.04	92.04 ± 0.02	<u>7.10</u> ± 0.70	<u>0.27</u> ± 0.01	1.143 ± 0.008	<u>32.17</u> ± 0.02
CF-5	100.0 ± 0.0	97.81 ± 0.01	91.98 ± 0.05	6.93 ± 0.32	<u>0.27</u> ± 0.01	1.087 ± 0.050	36.73 ± 0.03
EU-10	100.0 ± 0.0	97.87 ± 0.01	91.45 ± 0.07	13.30 ± 1.97	0.36 ± 0.02	0.849 ± 0.012	34.23 ± 0.02
CF-10	100.0 ± 0.0	97.87 ± 0.01	91.61 ± 0.05	15.80 ± 0.80	0.32 ± 0.02	0.734 ± 0.011	39.12 ± 0.0
SCRUB	100.0 ± 0.00	96.95 ± 0.03	92.12 ± 0.06	17.00 ± 1.21	<u>0.27</u> ± 0.02	<u>0.037</u> ± 0.036	17.84 ± 0.13
SALUN	99.73 ± 0.31	98.32 ± 0.04	92.23 ± 0.05	0.47 ± 0.06	0.78 ± 0.02	1.123 ± 0.043	203.12 ± 0.51
ℓ_1 -sparse	100.0 ± 0.0	<u>96.37</u> ± 0.06	<u>90.92</u> ± 0.07	3.80 ± 1.62	0.23 ± 0.01	1.144 ± 0.002	56.93 ± 0.32
COLA	100.0 ± 0.0	99.76 ± 0.02	90.23 ± 0.04	12.00 ± 2.20	0.54 ± 0.01	-0.022 ± 0.016	112.58 ± 0.82

Table 9: Multi-class forgetting on CIFAR-10 and CIFAR-100 datasets on ResNet-18 model. A better performance of an MU method corresponds to a smaller performance gap with Retrain (except RTE), with the top method in **bold** and the second best underlined.

CIFAR-10 - 2-class forgetting							
Methods	UA	RA	TA	MIA	JSD	IDI	RTE (min)
Original	0.0	100.0	95.76	91.10	3.55	1.000	170.32
Retrain	100.0	100.0	96.38	29.58	0.0	0.0	135.23
FT	99.98 \pm 0.01	100.0 \pm 0.0	96.36 \pm 0.09	0.96 \pm 0.53	0.58 \pm 0.08	0.750 \pm 0.009	5.92 \pm 0.09
RL	99.70 \pm 0.02	100.0 \pm 0.0	96.39 \pm 0.01	0.0 \pm 0.0	1.07 \pm 0.01	0.863 \pm 0.001	2.79 \pm 0.02
GA	99.07 \pm 0.38	99.43 \pm 0.13	94.83 \pm 0.22	26.71 \pm 3.68	0.42 \pm 0.02	0.612 \pm 0.001	3.72 \pm 0.13
Bad-T	99.96 \pm 0.05	100.0 \pm 0.0	95.33 \pm 0.09	67.47 \pm 34.59	3.98 \pm 1.08	1.010 \pm 0.005	4.40 \pm 0.20
EU-5	100.0 \pm 0.0	100.0 \pm 0.0	96.48 \pm 0.06	0.06 \pm 0.03	0.57 \pm 0.05	0.624 \pm 0.001	1.39 \pm 0.02
CF-5	80.06 \pm 8.26	100.0 \pm 0.0	96.70 \pm 0.04	0.0 \pm 0.0	0.80 \pm 0.02	0.781 \pm 0.006	<u>1.41</u> \pm 0.05
EU-10	100.0 \pm 0.0	99.67 \pm 0.02	94.94 \pm 0.17	25.92 \pm 0.79	<u>0.35</u> \pm 0.01	-0.011 \pm 0.011	<u>2.20</u> \pm 0.17
CF-10	100.0 \pm 0.0	99.67 \pm 0.02	94.94 \pm 0.17	21.20 \pm 1.43	<u>0.35</u> \pm 0.01	<u>0.221</u> \pm 0.007	2.19 \pm 0.14
SCRUB	99.98 \pm 0.0	<u>99.99</u> \pm 0.0	96.31 \pm 0.08	46.74 \pm 5.31	1.47 \pm 0.10	0.374 \pm 0.005	3.27 \pm 0.01
SALUN	95.86 \pm 4.18	<u>99.99</u> \pm 0.01	96.27 \pm 0.11	0.04 \pm 0.01	0.89 \pm 0.05	0.951 \pm 0.019	3.17 \pm 0.02
ℓ_1 -sparse	99.91 \pm 0.05	99.98 \pm 0.0	96.47 \pm 0.09	1.57 \pm 0.11	0.50 \pm 0.02	0.560 \pm 0.004	2.62 \pm 0.06
COLA	100.0 \pm 0.0	99.92 \pm 0.0	96.41 \pm 0.15	31.40 \pm 2.98	0.26 \pm 0.01	0.011 \pm 0.029	4.59 \pm 0.02
CIFAR-100 - 5-class forgetting							
Methods	UA	RA	TA	MIA	JSD	IDI	RTE (min)
Original	0.0	99.98	77.95	95.00	3.18	1.000	175.08
Retrain	100.0	99.98	78.45	7.12	0.0	0.0	165.92
FT	100.00 \pm 0.0	99.93 \pm 0.06	77.43 \pm 0.20	0.20 \pm 0.06	0.38 \pm 0.01	0.596 \pm 0.009	9.21 \pm 0.06
RL	98.61 \pm 0.22	99.98 \pm 0.0	77.78 \pm 0.19	0.0 \pm 0.0	0.71 \pm 0.01	0.613 \pm 0.008	3.39 \pm 0.09
GA	79.99 \pm 4.75	95.18 \pm 0.40	68.68 \pm 0.52	32.25 \pm 2.02	1.36 \pm 0.06	0.236 \pm 0.010	4.99 \pm 0.04
Bad-T	100.0 \pm 0.0	99.98 \pm 0.0	75.93 \pm 0.57	44.60 \pm 31.96	2.86 \pm 0.25	1.021 \pm 0.031	5.51 \pm 0.11
EU-5	100.0 \pm 0.0	99.75 \pm 0.02	75.14 \pm 0.12	12.40 \pm 0.26	0.54 \pm 0.01	<u>0.054</u> \pm 0.010	2.01 \pm 0.0
CF-5	100.0 \pm 0.0	<u>99.97</u> \pm 0.0	77.36 \pm 0.06	<u>3.37</u> \pm 0.52	<u>0.36</u> \pm 0.02	0.319 \pm 0.011	<u>2.10</u> \pm 0.0
EU-10	100.0 \pm 0.0	91.76 \pm 0.12	73.24 \pm 0.11	21.96 \pm 0.49	0.48 \pm 0.01	-0.155 \pm 0.008	4.25 \pm 0.0
CF-10	100.0 \pm 0.0	99.88 \pm 0.01	76.59 \pm 0.24	10.69 \pm 1.29	0.40 \pm 0.01	0.087 \pm 0.019	4.29 \pm 0.01
SCRUB	100.0 \pm 0.0	<u>99.97</u> \pm 0.0	<u>77.64</u> \pm 0.11	0.95 \pm 0.35	0.56 \pm 0.03	0.289 \pm 0.015	2.27 \pm 0.03
SALUN	100.0 \pm 0.0	99.96 \pm 0.01	77.18 \pm 0.14	0.13 \pm 0.09	0.55 \pm 0.01	0.597 \pm 0.029	4.46 \pm 0.04
ℓ_1 -sparse	<u>98.63</u> \pm 0.37	97.50 \pm 0.14	73.46 \pm 0.25	12.35 \pm 0.82	0.38 \pm 0.01	0.196 \pm 0.011	4.19 \pm 0.01
COLA	100.0 \pm 0.0	99.82 \pm 0.0	77.47 \pm 0.26	11.16 \pm 0.54	0.29 \pm 0.01	0.044 \pm 0.010	7.31 \pm 0.02
CIFAR-100 - 20-class forgetting							
Methods	UA	RA	TA	MIA	JSD	IDI	RTE (min)
Original	0.0	99.97	78.03	95.04	3.15	1.000	175.08
Retrain	100.0	99.98	80.01	7.55	0.0	0.0	139.93
FT	99.81 \pm 0.04	<u>99.97</u> \pm 0.00	79.11 \pm 0.35	0.22 \pm 0.05	0.37 \pm 0.01	<u>0.474</u> \pm 0.007	7.43 \pm 0.07
RL	95.77 \pm 0.09	99.98 \pm 0.01	78.42 \pm 0.05	0.0 \pm 0.0	0.63 \pm 0.01	1.207 \pm 0.004	2.94 \pm 0.01
GA	67.06 \pm 2.58	96.65 \pm 0.47	70.80 \pm 0.65	30.16 \pm 1.42	1.46 \pm 0.11	1.027 \pm 0.006	4.11 \pm 0.02
Bad-T	95.54 \pm 0.61	99.98 \pm 0.01	69.71 \pm 0.32	32.07 \pm 35.23	2.83 \pm 0.26	1.211 \pm 0.011	5.17 \pm 0.11
EU-5	100.0 \pm 0.0	99.82 \pm 0.02	76.89 \pm 0.03	14.50 \pm 0.54	0.52 \pm 0.01	0.807 \pm 0.003	<u>1.83</u> \pm 0.04
CF-5	100.0 \pm 0.0	99.96 \pm 0.02	<u>78.82</u> \pm 0.06	2.68 \pm 0.21	<u>0.33</u> \pm 0.01	1.060 \pm 0.008	1.80 \pm 0.03
EU-10	100.0 \pm 0.0	93.25 \pm 0.32	74.79 \pm 0.39	25.63 \pm 0.38	0.47 \pm 0.01	0.617 \pm 0.005	3.61 \pm 0.51
CF-10	100.0 \pm 0.0	99.91 \pm 0.01	78.39 \pm 0.24	13.57 \pm 0.32	0.39 \pm 0.01	0.889 \pm 0.005	3.68 \pm 0.16
SCRUB	95.03 \pm 0.75	99.90 \pm 0.00	77.61 \pm 0.07	0.93 \pm 0.13	0.38 \pm 0.01	0.997 \pm 0.007	2.14 \pm 0.02
SALUN	90.69 \pm 0.76	98.97 \pm 0.14	74.72 \pm 0.54	0.17 \pm 0.03	0.60 \pm 0.01	1.113 \pm 0.008	3.85 \pm 0.0
ℓ_1 -sparse	83.49 \pm 0.46	99.52 \pm 0.03	76.79 \pm 0.20	6.36 \pm 0.59	0.38 \pm 0.01	1.035 \pm 0.007	3.08 \pm 0.07
COLA	100.0 \pm 0.0	99.92 \pm 0.0	78.59 \pm 0.32	<u>11.52</u> \pm 0.39	0.24 \pm 0.01	0.007 \pm 0.010	6.97 \pm 0.01

Table 10: 5-class forgetting results on ImageNet-1K dataset across different model architectures. A better performance of an MU method corresponds to a smaller performance gap with Retrain (except RTE), with the top method in **bold** and the second best underlined. The \star symbol indicated in RTE of Original and Retrain means that models are pretrained on ImageNet-21K and then finetuned on ImageNet-1K, with the reported time reflecting only the finetuning process. In contrast, Original and Retrain without \star are trained from scratch on ImageNet-1K.

ImageNet-1K - ResNet-50							
Methods	UA	RA	TA	MIA	JSD	IDI	RTE (min)
Original	11.72	87.45	76.11	61.69	3.73	1.000	2680.15
Retrain	100.0	88.80	75.88	9.41	0.0	0.0	2661.90
FT	100.0 ± 0.0	88.52 ± 0.0	<u>76.16</u> ± 0.01	8.24 ± 1.23	<u>0.24</u> ± 0.01	0.102 ± 0.026	140.04 ± 1.42
RL	<u>99.96</u> ± 0.03	86.46 ± 0.07	<u>75.23</u> ± 0.01	0.23 ± 0.01	1.57 ± 0.03	1.002 ± 0.007	200.73 ± 1.87
GA	100.0 ± 0.0	80.77 ± 0.22	71.49 ± 0.10	4.20 ± 0.46	0.42 ± 0.03	0.328 ± 0.023	212.14 ± 2.61
Bad-T	98.01 ± 0.02	84.03 ± 0.03	73.42 ± 0.03	69.13 ± 12.57	3.51 ± 0.41	1.152 ± 0.072	211.52 ± 0.96
EU-5	100.0 ± 0.0	79.62 ± 0.0	71.22 ± 0.13	13.33 ± 1.53	0.26 ± 0.01	0.183 ± 0.028	193.38 ± 0.78
CF-5	100.0 ± 0.0	84.31 ± 0.08	74.16 ± 0.06	10.21 ± 5.33	0.23 ± 0.01	0.701 ± 0.014	81.53 ± 0.56
EU-10	100.0 ± 0.0	71.84 ± 0.03	65.78 ± 0.02	16.65 ± 1.91	0.35 ± 0.04	<u>-0.051</u> ± 0.021	193.79 ± 0.47
CF-10	100.0 ± 0.0	80.87 ± 0.04	72.34 ± 0.08	13.99 ± 5.41	0.25 ± 0.01	0.608 ± 0.012	<u>82.29</u> ± 0.34
SCRUB	99.28 ± 0.07	<u>88.39</u> ± 0.04	76.51 ± 0.03	7.42 ± 0.51	0.25 ± 0.01	0.517 ± 0.011	426.04 ± 2.98
SALUN	89.67 ± 0.27	86.25 ± 0.15	75.54 ± 0.10	0.50 ± 0.09	0.88 ± 0.01	0.343 ± 0.017	793.82 ± 3.32
ℓ_1 -sparse	97.57 ± 0.61	85.33 ± 0.07	74.77 ± 0.03	<u>8.84</u> ± 1.39	0.32 ± 0.02	0.239 ± 0.031	226.74 ± 1.35
COLA	100.0 ± 0.0	87.93 ± 0.05	76.15 ± 0.04	9.95 ± 1.21	<u>0.24</u> ± 0.01	0.040 ± 0.042	171.44 ± 0.75
ImageNet-1K - ViT							
Methods	UA	RA	TA	MIA	JSD	IDI	RTE (min)
Original	2.48	98.18	80.59	71.00	4.45	1.000	1943.69 \star
Retrain	100.0	98.33	80.42	8.09	0.0	0.0	1920.77 \star
FT	96.39 ± 0.01	98.85 ± 0.03	80.93 ± 0.06	3.88 ± 0.33	0.65 ± 0.02	0.937 ± 0.009	281.73 ± 2.30
RL	98.33 ± 0.02	98.99 ± 0.07	81.65 ± 0.07	0.0 ± 0.0	2.13 ± 0.15	1.152 ± 0.033	150.32 ± 4.31
GA	100.0 ± 0.0	97.04 ± 0.01	<u>80.17</u> ± 0.04	8.26 ± 2.14	0.52 ± 0.23	0.674 ± 0.021	193.73 ± 2.23
Bad-T	98.21 ± 0.03	<u>97.85</u> ± 0.07	80.58 ± 0.03	0.0 ± 0.0	2.62 ± 0.06	1.312 ± 0.015	721.15 ± 5.23
EU-5	100.0 ± 0.0	93.82 ± 0.02	80.00 ± 0.01	4.74 ± 1.33	0.63 ± 0.02	0.519 ± 0.008	300.55 ± 0.76
CF-5	98.75 ± 0.0	96.57 ± 0.01	80.09 ± 0.04	4.49 ± 0.34	0.64 ± 0.01	0.731 ± 0.024	122.39 ± 0.53
EU-10	100.0 ± 0.0	87.33 ± 0.10	76.26 ± 0.13	8.09 ± 0.20	0.36 ± 0.02	-2.662 ± 0.231	345.37 ± 0.70
CF-10	<u>99.95</u> ± 0.01	93.86 ± 0.02	78.69 ± 0.01	7.68 ± 1.11	0.72 ± 0.03	<u>0.009</u> ± 0.021	<u>140.11</u> ± 0.49
SCRUB	100.0 ± 0.00	98.84 ± 0.02	81.62 ± 0.01	3.19 ± 0.91	1.062 ± 0.03	-0.846 ± 0.032	404.02 ± 2.96
SALUN	94.64 ± 0.76	98.13 ± 0.21	80.74 ± 0.05	0.13 ± 0.01	1.83 ± 0.09	0.980 ± 0.065	321.13 ± 2.75
ℓ_1 -sparse	93.55 ± 0.62	94.69 ± 0.37	78.84 ± 0.10	2.98 ± 0.33	<u>0.49</u> ± 0.01	0.831 ± 0.022	717.42 ± 3.21
COLA	100.0 ± 0.0	96.42 ± 0.03	79.28 ± 0.21	<u>8.02</u> ± 1.36	0.59 ± 0.02	0.006 ± 0.007	501.12 ± 2.17

Table 11: Random data forgetting on CIFAR-10 and CIFAR-100 datasets on ResNet-18 model. A better performance of an MU method corresponds to a smaller performance gap with Retrain (except RTE), with the top method in **bold** and the second best underlined.

CIFAR-10 - ResNet-18							
Methods	UA	RA	TA	MIA	JSD	IDI	RTE (min)
Original	0.0	100.0	95.54	92.90	0.09	1.000	170.32
Retrain	3.94	100.0	95.26	75.12	0.0	0.0	152.87
FT	5.03 \pm 0.40	98.95 \pm 0.21	92.94 \pm 0.26	83.52 \pm 0.58	0.07 \pm 0.11	<u>-0.069</u> \pm 0.013	8.11 \pm 0.03
RL	4.77 \pm 0.27	99.92 \pm 0.0	93.54 \pm 0.04	22.47 \pm 1.19	0.38 \pm 0.02	0.084 \pm 0.030	2.75 \pm 0.01
GA	2.86 \pm 0.76	98.37 \pm 0.71	91.90 \pm 0.70	85.49 \pm 2.17	0.09 \pm 0.01	0.924 \pm 0.028	4.31 \pm 0.03
Bad-T	5.47 \pm 1.05	<u>99.87</u> \pm 0.05	91.51 \pm 0.61	39.53 \pm 3.43	0.27 \pm 0.03	0.939 \pm 0.053	4.78 \pm 0.09
EU-10	3.16 \pm 0.19	98.68 \pm 0.08	93.07 \pm 0.12	<u>83.40</u> \pm 0.21	<u>0.06</u> \pm 0.01	-0.110 \pm 0.013	<u>2.13</u> \pm 0.05
CF-10	2.71 \pm 0.24	99.11 \pm 0.06	<u>93.47</u> \pm 0.15	84.33 \pm 0.05	0.05 \pm 0.01	0.219 \pm 0.029	2.10 \pm 0.06
SCRUB	<u>4.31</u> \pm 1.50	96.21 \pm 1.70	88.83 \pm 1.86	37.88 \pm 7.65	0.56 \pm 0.09	0.322 \pm 0.016	3.37 \pm 0.05
SALUN	2.74 \pm 0.30	97.77 \pm 0.04	91.68 \pm 0.44	83.52 \pm 2.20	0.10 \pm 0.03	0.861 \pm 0.012	5.69 \pm 0.04
ℓ_1 -sparse	5.47 \pm 0.22	96.66 \pm 0.07	91.31 \pm 0.25	77.12 \pm 0.21	0.09 \pm 0.01	-0.157 \pm 0.026	3.03 \pm 0.04
COLA+	3.90 \pm 0.08	99.24 \pm 0.17	93.23 \pm 0.09	83.48 \pm 0.10	<u>0.06</u> \pm 0.01	0.024 \pm 0.010	7.80 \pm 0.02
CIFAR-100 - ResNet-18							
Methods	UA	RA	TA	MIA	JSD	IDI	RTE (min)
Original	0.0	99.98	78.09	95.82	0.56	1.000	175.08
Retrain	23.10	99.98	77.78	39.72	0.0	0.0	0.0
FT	17.44 \pm 1.12	98.46 \pm 0.24	70.99 \pm 0.45	67.35 \pm 0.53	0.46 \pm 0.02	0.311 \pm 0.034	8.40 \pm 0.13
RL	24.67 \pm 0.42	<u>99.66</u> \pm 0.0	73.10 \pm 0.49	2.13 \pm 0.17	0.84 \pm 0.02	-0.246 \pm 0.056	2.95 \pm 0.03
GA	11.73 \pm 1.43	95.21 \pm 0.78	68.38 \pm 1.03	74.97 \pm 1.10	0.65 \pm 0.01	0.704 \pm 0.039	4.66 \pm 0.03
Bad-T	64.35 \pm 7.44	99.07 \pm 0.56	53.05 \pm 2.53	11.85 \pm 5.93	1.51 \pm 0.16	1.003 \pm 0.006	5.04 \pm 0.05
EU-10	24.15 \pm 0.09	90.15 \pm 0.08	72.25 \pm 0.36	59.47 \pm 0.39	0.27 \pm 0.01	0.404 \pm 0.085	<u>2.31</u> \pm 0.02
CF-10	20.40 \pm 0.20	95.06 \pm 0.24	74.44 \pm 0.23	62.18 \pm 0.27	<u>0.25</u> \pm 0.01	0.464 \pm 0.061	2.30 \pm 0.02
SCRUB	3.47 \pm 2.85	97.77 \pm 2.31	71.89 \pm 2.87	71.49 \pm 4.15	0.37 \pm 0.02	0.528 \pm 0.013	3.59 \pm 0.05
SALUN	32.77 \pm 1.20	99.87 \pm 0.02	71.97 \pm 0.37	3.32 \pm 0.28	0.81 \pm 0.02	<u>-0.226</u> \pm 0.078	5.99 \pm 0.09
ℓ_1 -sparse	22.83 \pm 0.15	88.94 \pm 0.41	69.54 \pm 0.73	62.36 \pm 0.37	0.26 \pm 0.01	0.634 \pm 0.072	3.37 \pm 0.03
COLA+	<u>23.50</u> \pm 0.16	93.78 \pm 0.07	<u>73.15</u> \pm 0.59	<u>59.58</u> \pm 0.24	0.24 \pm 0.01	0.078 \pm 0.013	10.2 \pm 0.16

Table 12: Standard Deviation of Figure 5 - (CIFAR-10, ResNet-18)

Method	Block 1	Block 2	Block 3	Block 4	Block 5	IDI
Original	0.002	0.002	0.003	0.006	0.006	0.005
Retrain	0.001	0.003	0.003	0.006	0.007	0.007
FT	0.001	0.002	0.004	0.010	0.008	0.007
RL	0.002	0.004	0.005	0.003	0.005	0.004
GA	0.001	0.001	0.004	0.006	0.011	0.013
l1-sparse	0.001	0.000	0.002	0.007	0.007	0.011
SCRUB	0.001	0.005	0.003	0.004	0.005	0.007
SALUN	0.002	0.001	0.003	0.005	0.012	0.011

Table 13: Standard Deviation of Figure 5 - (CIFAR-10, ResNet-50)

Method	Block 1	Block 2	Block 3	Block 4	Block 5	Block 6	IDI
Original	0.003	0.002	0.009	0.007	0.013	0.008	0.011
Retrain	0.001	0.003	0.001	0.008	0.005	0.007	0.009
FT	0.003	0.005	0.008	0.015	0.011	0.012	0.019
RL	0.005	0.005	0.007	0.003	0.008	0.004	0.009
GA	0.002	0.001	0.003	0.011	0.010	0.013	0.018
l1-sparse	0.002	0.004	0.002	0.004	0.021	0.015	0.023
SCRUB	0.000	0.004	0.004	0.023	0.028	0.031	0.060
SALUN	0.001	0.000	0.006	0.005	0.020	0.011	0.019

Table 14: Standard Deviation of Figure 8

Method	Ratio 1:5	Ratio 1:20	Ratio 1:99
FT	0.013	0.008	0.019
RL	0.016	0.007	0.009
GA	0.020	0.008	0.018
CF-10	0.007	0.016	0.035
SALUN	0.023	0.025	0.019
SCRUB	0.006	0.013	0.023

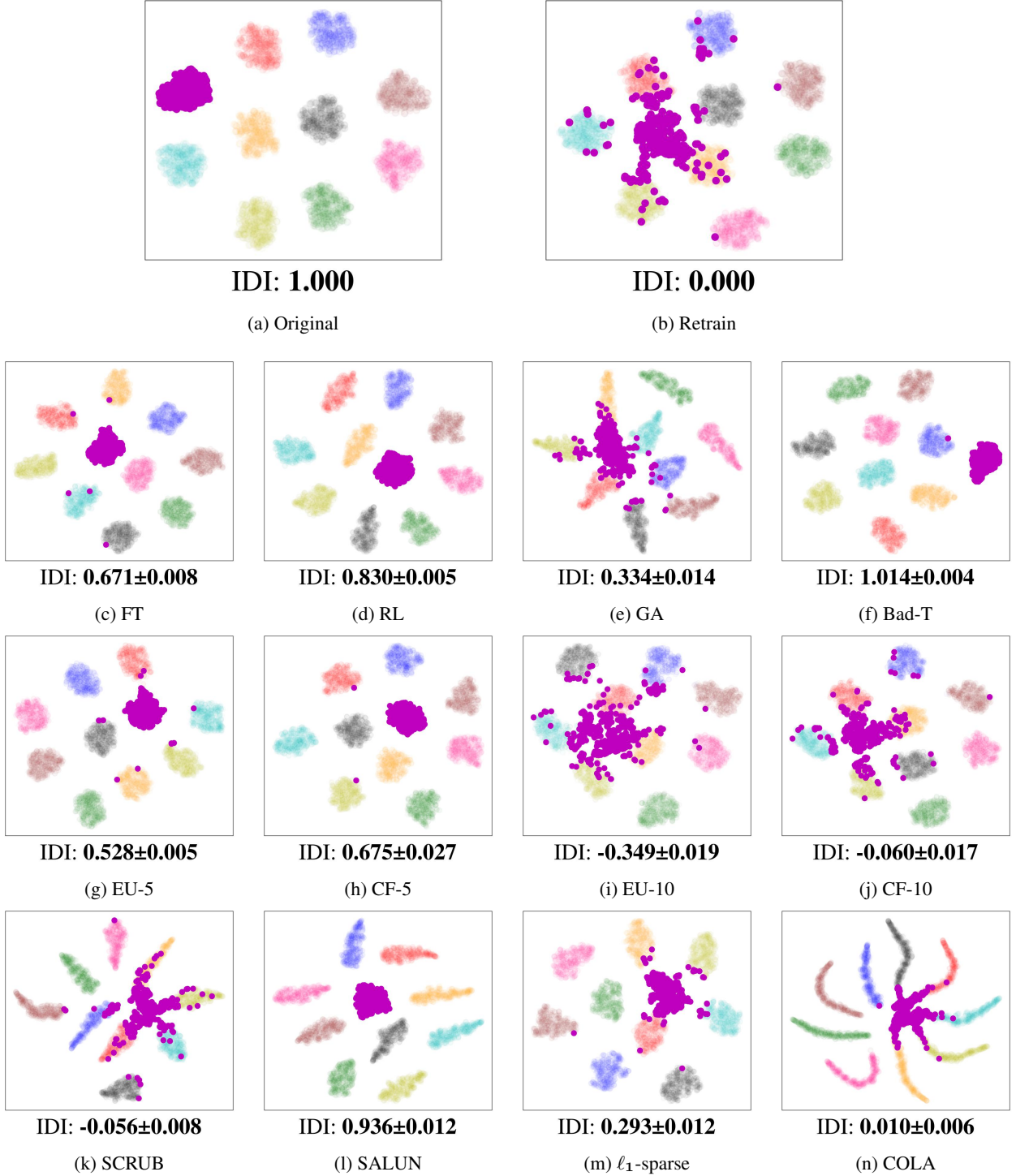


Figure 11: t-SNE visualizations of features of Original, Retrain, and unlearned models (FT, RL, GA, Bad-T, EU-5, CF-5, EU-10, CF-10, SCRUB, SALUN, ℓ_1 -sparse, and COLA) on CIFAR-10 with ResNet-18. The forgetting class is represented in purple, while rest of the points represents the remaining class.

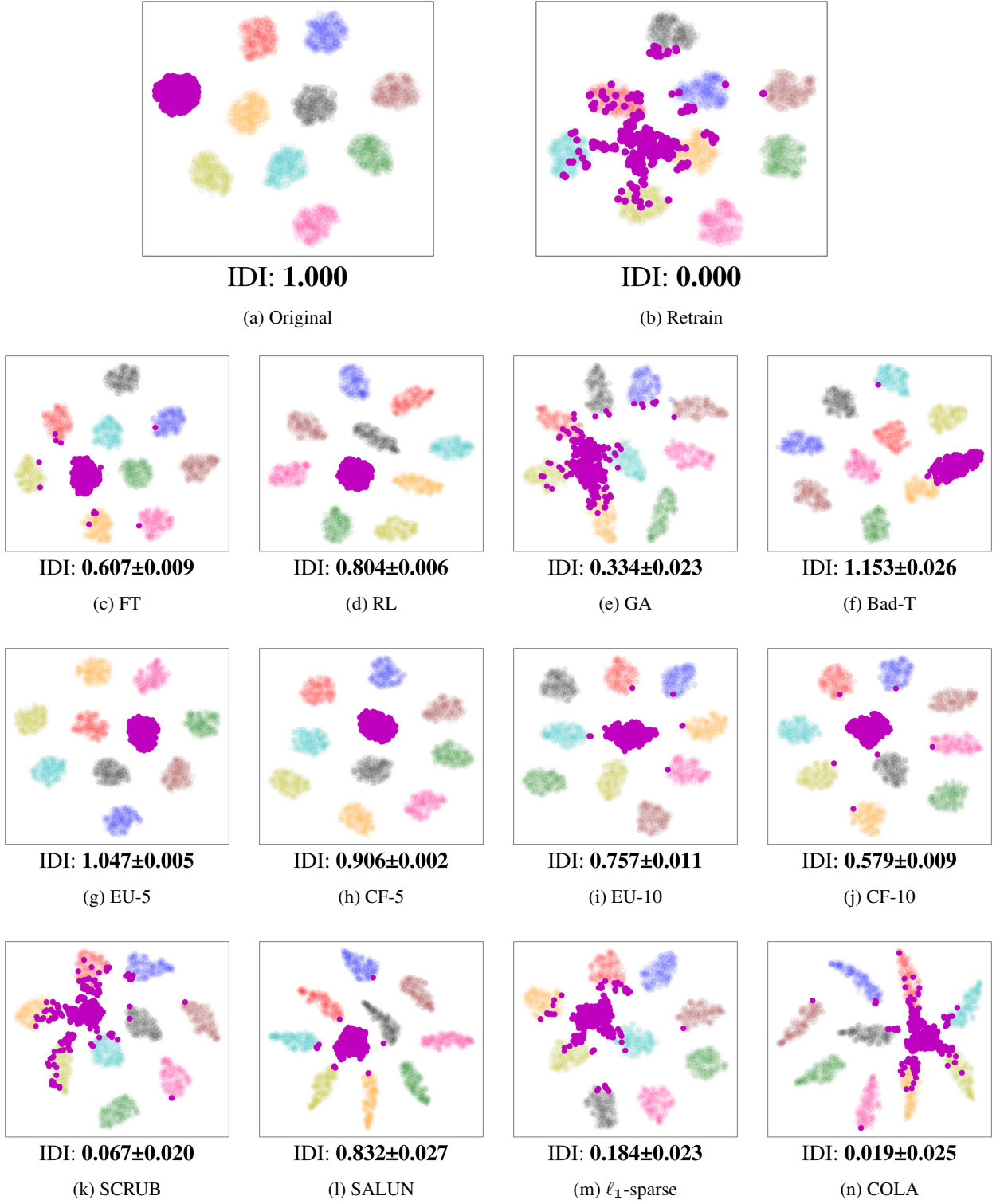


Figure 12: t-SNE visualizations of feature of Original, Retrain, and unlearned models (FT, RL, GA, Bad-T, EU-5, CF-5, EU-10, CF-10, SCRUB, SALUN, ℓ_1 -sparse, and COLA) on CIFAR-10 with ResNet-50. The forgetting class is represented in purple, while rest of the points represents the remaining class.

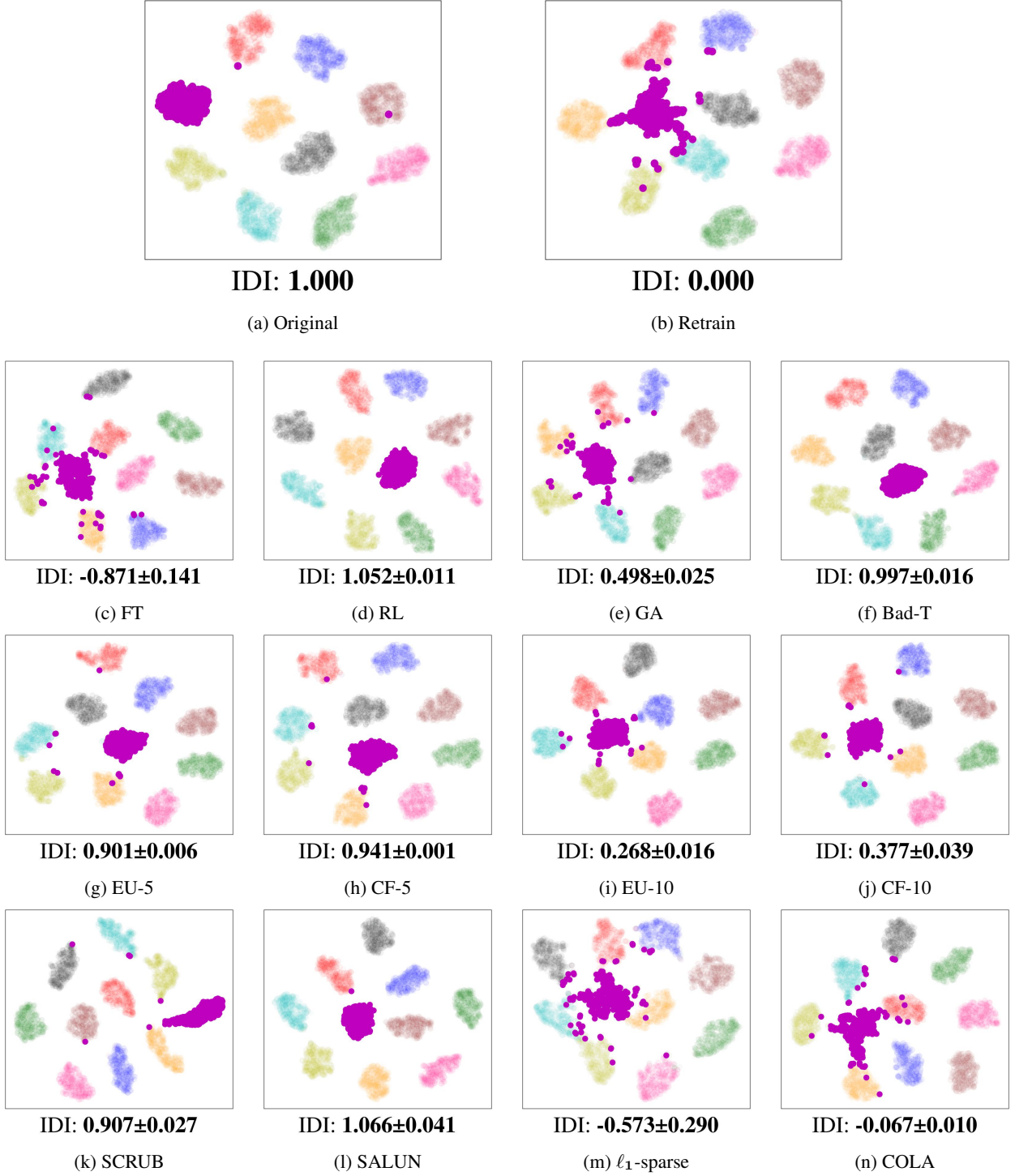
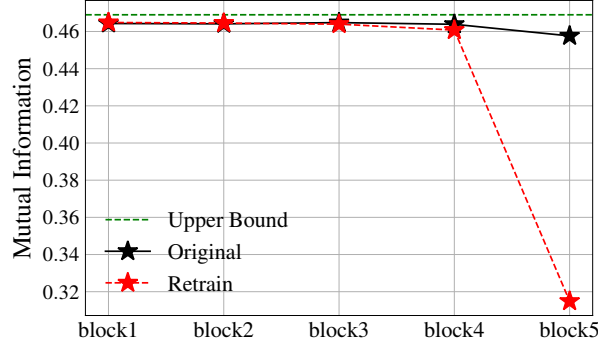
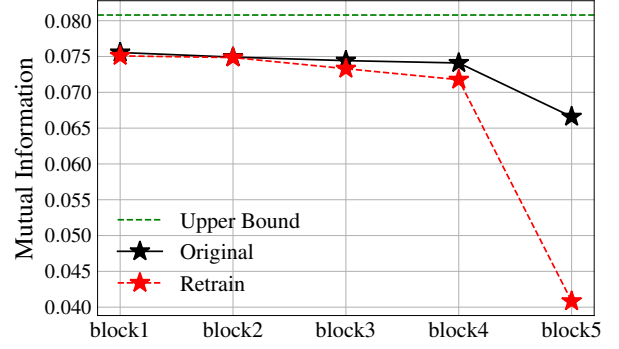


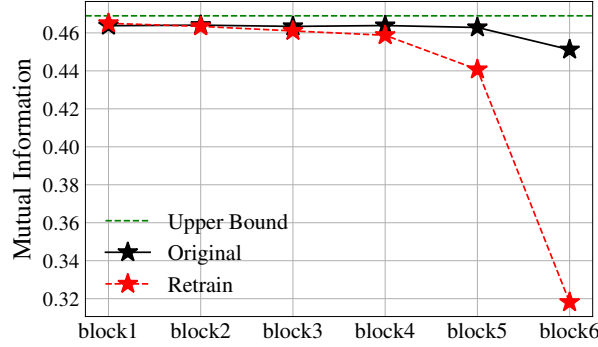
Figure 13: t-SNE visualizations of features of Original, Retrain, and unlearned models (FT, RL, GA, Bad-T, EU-5, CF-5, EU-10, CF-10, SCRUB, SALUN, ℓ_1 -sparse, and COLA) on CIFAR-10 with ViT. The forgetting class is represented in purple, while rest of the points represents the remaining class.



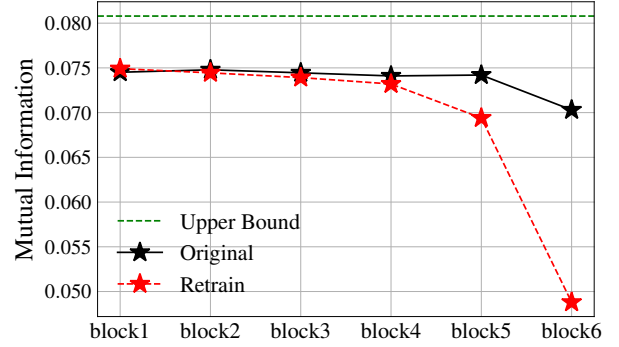
(a) CIFAR-10 - ResNet-18



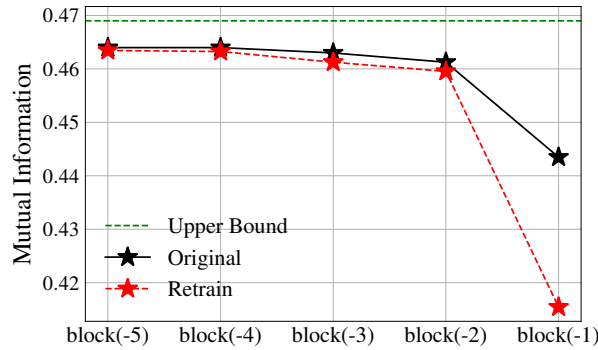
(b) CIFAR-100 - ResNet-18



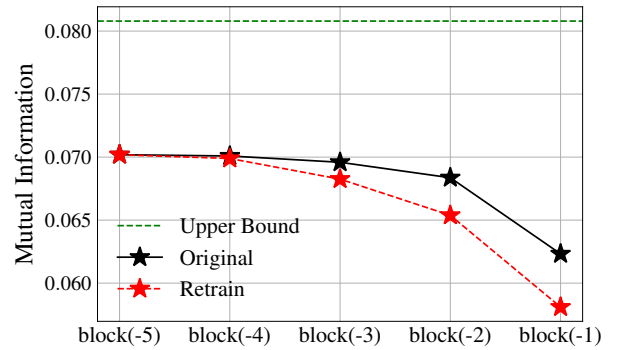
(c) CIFAR-10 - ResNet-50



(d) CIFAR-100 - ResNet-50



(e) CIFAR-10 - ViT



(f) CIFAR-100 - ViT

Figure 14: Mutual information curves across various datasets and model architectures. It illustrates the estimated mutual information $I(\mathbf{Z}_\ell; Y)$ of the features from the ℓ -th layer \mathbf{Z}_ℓ and the binary label Y , computed by the InfoNCE loss. ‘block(-k)’ means the k block front from the last layer.

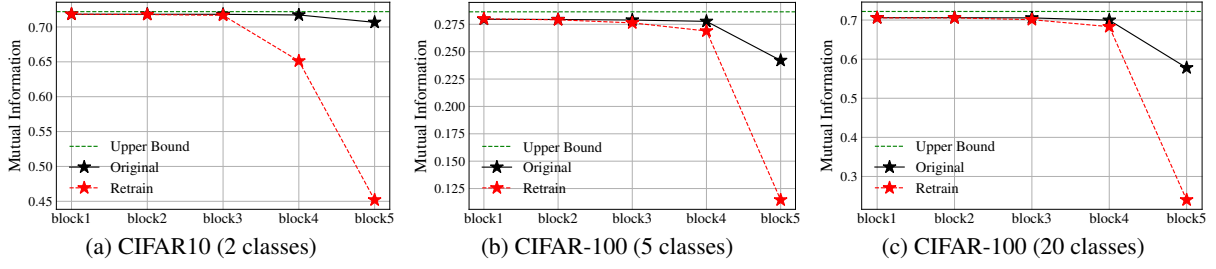


Figure 15: Mutual information curves for multiple class unlearning in ResNet-18 architecture. It illustrates the estimated mutual information $I(\mathbf{Z}_\ell; Y)$ of the features from the ℓ -th layer \mathbf{Z}_ℓ and the binary label Y , computed by the InfoNCE loss.

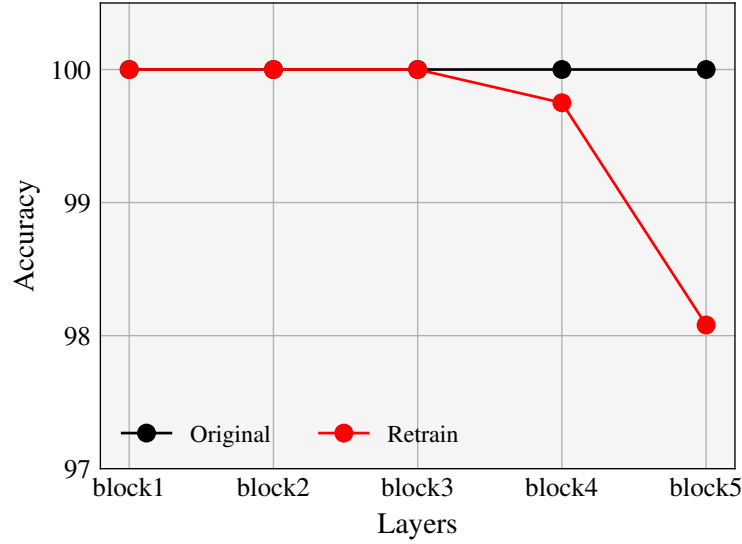


Figure 16: Binary train accuracy on CIFAR-10 in single-class forgetting with retain and forget sets. Interestingly, it shows similar results with mutual information plots shown Figure 14.

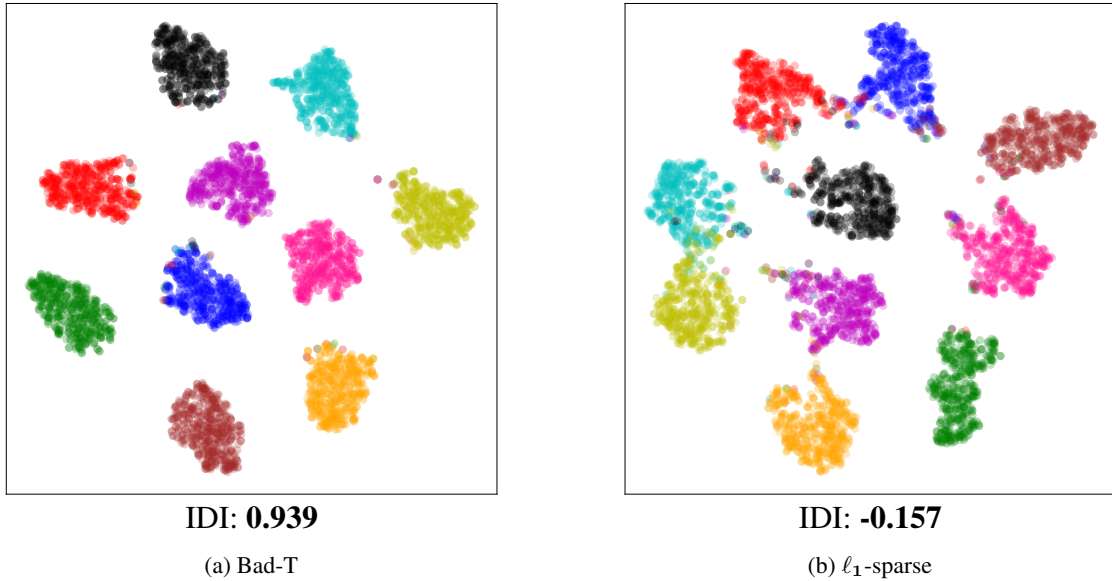


Figure 17: t-SNE visualizations of features of forget samples of Bad-T and ℓ_1 -sparse in a random data forgetting task on (CIFAR-10, ResNet-18). The clusters of ℓ_1 -sparse are more disperse than those of Bad-T.